9 Ultrasound for Characterizing Emulsions and Microemulsions

A.S. Dukhin and P.J. Goetz

CONTENTS

Abstract

Ultrasound-based techniques (acoustics and electroacoustics) offer a unique opportunity to characterize concentrated emulsions and microemulsions in their natural state, without dilution. Elimination of the dilution protocol is crucial for an adequate characterization of liquid dispersions as dilution can change the thermodynamic equilibrium in these systems.

In this review, we present a short review of theoretical basis for the mentioned ultrasound techniques. Emphasis is placed on the mechanism of thermal losses, which is related to the thermodynamic properties of liquids and dominates ultrasound attenuation of many emulsions, microemulsions, and latex systems.

There are already many examples when this theoretical model allows us to achieve a successful characterization of various liquid-based systems. It is incorporated into the software of commercially available instruments made by Dispersion Technology Inc. In this review, we present several of these examples.

The first application is characterization of various dairy products. We show that acoustic attenuation technique is able to provide reliable information on the milk fat droplet size in milks, as well as a droplet size of water in butter. In addition this method might be suitable for characterizing fat content of dairy products.

The second application presents our recent observation of the evolution of the water-in-kerosene system from emulsion to mini-emulsion state. We show how ultrasound-based techniques allow us to monitor the kinetics of droplet size variation and reveal the reason for this variation. We show that the droplet size could be controlled by ion exchange between water droplets and the bulk of nonpolar liquid.

The third application presents characterization of microemulsions. We show how concentration of surfactant determines the water droplet size distribution in hexadecane. These results are in a very good agreement with independent measurements by X-ray and neutron scattering.

9.1 INTRODUCTION

The widespread acceptance and commercialization of acoustic spectroscopy has been slow to develop. This technique has been overlooked by many in academia and industry in the past, but has recently been showing increased levels of acceptance. This powerful method of characterizing concentrated heterogeneous systems has all the capabilities for being successful.

The first hardware for measuring acoustic properties of liquids was developed more than 50 years ago at MIT [1] by Pellam and Galt. The first acoustic theory for heterogeneous systems was created by Sewell 90 years ago [2]. Epstein and Carhart formulated the general principles of the acoustic theory 50 years ago [3]. There is a long list of applications and experiments using acoustic spectroscopy presented in recent publications [4–6].

Acoustics is able to provide reliable particle size information for concentrated dispersions without any dilution. There are examples when acoustics yields size information at volume fractions above 40%. This in-situ characterization of concentrated systems makes the acoustic method very useful and unique in this capability compared to alternate methods, including light scattering, where dilution is required.

Acoustics is also able to deal with low dispersed phase volume fractions and in some systems can characterize down to below 0.1% vol. This flexibility for concentration range provides an overlap with classic methods for dilute systems. In the overlap range, acoustics size characterization has been found to have excellent agreement with these other techniques [6].

Many people have perceived acoustics to have a high degree of complexity. The operating principles are in fact quite straightforward. The acoustic spectrometer generates sound pulses that pass through a sample system and are then measured by a receiver. The passage through the sample system causes the sound energy to change in intensity and phase. The acoustic instrument measures the sound energy losses (attenuation) and the sound speed. The sound attenuates due to the interaction with the particles and liquid in the sample system. Acoustic spectrometers generally operate with sound in the frequency range of 1 to 100 MHz. This is a much higher sound frequency than the upper limit of our hearing, which is only 0.02 MHz.

While the operating principles are relatively simple, the analysis of the attenuation data to obtain particle size distributions does involve a degree of complexity in fitting experimental results to theoretical models based on various acoustic loss mechanisms. The advent of high-speed computers and the refinement of these theoretical models have made the inherent complexity of this analysis of little consequence. In comparison, many other particle sizing techniques such as photon correlation spectroscopy also rely on similar levels of complexity in analyzing experimental results.

Acoustics is not only a particle sizing technique, but also provides information about the microstructure of the dispersed system. The acoustic spectrometer can be considered as a micro-rheometer. In acoustics, stresses are applied in the same way as regular rheometers, but over a very short distance on the micron scale. In this way, the microstructure of the dispersed system can be sensed. Currently, this feature of the acoustics is only beginning to be exploited, but it is certainly very promising.

In addition to characterizing special heterogeneity and structural properties, ultrasound offers an opportunity for studying electric surface properties of concentrated emulsions. There is a related field that is usually referred to as "electroacoustics" [7–9]. Electroacoustics can provide information on the zeta potential and surface charge of the droplets. This relatively new technique is more complex than acoustics because an additional electric field is involved. As a result, both hardware and theory become more complicated. There are even two different versions of electroacoustics depending on what field is used as a driving force. Electrokinetic sonic amplitude (ESA) involves the generation of sound energy caused by the driving force of an applied electric field. Colloid vibration current (CVC) is a phenomenon when sound energy is applied to a system. This results in electric field or current created by the vibration of the droplets' electric double layers.

Coming back to acoustics, its lack of widespread acceptance may be related to the fact that it yields too much, sometimes overwhelming, information. Instead of dealing with interpretation of the acoustic spectra it is often easier to dilute the system of interest and apply light-based techniques. It was often naïvely assumed that the dilution had not affected the emulsion characteristics. Lately, many researchers are coming to the realization that emulsion systems need to be analyzed in their natural concentrated form, and that dilution destroys many useful and important properties.

We are optimistic about the future of acoustics in colloid science. It is amazing what this technique can do especially in combination with electroacoustics for characterizing electric surface properties. We hope that this review will provide additional information concerning the power and opportunities related to these sound-based techniques.

9.2 THEORETICAL BACKGROUND

There are six known mechanisms of ultrasound interaction with a dispersed system:

- Viscous
- Thermal
- Scattering
- Intrinsic
- Structural
- Electrokinetic

Here we give only short qualitative descriptions omitting complicated mathematical models.

Viscous losses of the acoustic energy occur due to the shear waves generated by the particle oscillating in the acoustic pressure field. These shear waves appear because of the difference in the densities of the particles and medium. This density contrast causes the particle motion with respect to the medium. As a result, the liquid layers in the particle vicinity slide relative to each other. This sliding non-stationary motion of the liquid near the particle is referred to as the "shear wave." Viscous losses are dominant for small rigid particles with sizes below 3 microns, such as oxides, pigments, paints, ceramics, cement, and graphite.

The reason for the *thermal losses* is the temperature gradients generated near the particle surface. These temperature gradients are due to the thermodynamic coupling between pressure and temperature. This mechanism is dominant for soft particles, including emulsion droplets and latex beads.

The mechanism of the *scattering losses* is quite different than the viscous and thermal losses. Acoustic scattering does not produce dissipation of acoustic energy. This scattering mechanism is similar to light scattering. Particles simply redirect a part of the acoustic energy flow and as a result this portion of the sound does not reach the sound transducer. This mechanism is important for larger particles (>3 micron) and high frequency (>10 MHz).

The *intrinsic losses* of the acoustic energy occur due to the interaction of the sound wave with the materials of the particles and medium as homogeneous phases on a molecular level.

Structural losses are caused by the oscillation of a network of particles that are interconnected. Thus, this mechanism is specific for the given type of structured system.

Electrokinetic losses are caused by the oscillation of charged particles in an acoustic field that leads to the generation of an alternating electrical field, and consequently to alternating electric current. As a result, a part of the acoustic energy is transformed into electric energy and then irreversibly to heat.

Only the first four loss mechanisms (viscous, thermal, scattering, and intrinsic) make a significant contribution to the overall attenuation spectra in most cases. Structural losses are significant only in structured systems that require a quite different theoretical framework. These four mechanisms form the basis for acoustic spectroscopy.

The contribution of electrokinetic losses to the total sound attenuation is almost always negligibly small [10] and will be neglected. This opens an opportunity to separate acoustic spectroscopy from electroacoustic spectroscopy because the acoustic attenuation spectrum is independent of the electric properties of the dispersed system. Following this distinction between acoustics and electroacoustics, the corresponding theories will be considered separately.

9.2.1 Theory of Acoustics

The most well known acoustic theory for heterogeneous systems was developed by Epstein and Carhart [3]. Later Allegra and Hawley [11] made some important modifications. The resulting general theory has abbreviated to ECAH theory. This theory takes into account the four most important mechanisms (viscous, thermal, scattering, and intrinsic). This theory describes attenuation for a monodisperse system of spherical particles and is valid only for dilute systems.

The term "monodisperse" assumes that all of the particles have the same diameter. Extensions of the ECAH theory to include polydispersity have typically assumed a simple linear superposition of the attenuation for each size fraction. The term "spherical" is used to denote that all calculations are performed assuming that each particle can be adequately represented as a sphere.

Most importantly, the term "dilute" is used to indicate that there is no consideration of particle–particle interactions. This fundamental limitation normally restricts the application of the resultant theory to dispersions with a volume fraction of less than a few volume percent. However, there is some evidence that the ECAH theory, in some very specific situations, does nevertheless provide a correct interpretation of experimental data, even for volume fractions as large as 30%.

Allegra and Hawley provided the earliest demonstration of this ability of the ECAH theory. They observed almost perfect correlation between experiment and dilute case ECAH theory for several systems: a 20% by volume toluene emulsion; a 10% by volume hexadecane emulsion; and a 10% by volume polystyrene latex. Similar work with emulsions by McClements [12,13] has

provided similar results. The recent work by Holmes, Challis, and Wedlock [14,15] shows good agreement between ECAH theory and experiments even for 30% by volume polystyrene latex.

A surprising absence of particle–particle interaction was observed with neoprene latex [16]. This experiment showed that attenuation is linear function of the volume fraction up to 30% for this particular system. This linearity is an indication that each particle fraction contributes to the total attenuation independently of other fractions, and is a superposition of individual contributions. Superposition works only when particle–particle interaction is insignificant.

It is important to note that the surprising validity of the dilute ECAH theory for moderately concentrated systems has only been demonstrated in systems where the "thermal losses" were dominant, such as emulsions and latex systems. In contrast, the solid rutile dispersion exhibits non-linearity of the attenuation above 10% by volume [6].

The difference between the "viscous depth" and the "thermal depth" provides an answer to the observed differences between emulsions and solid particle dispersions. These parameters characterize the penetration of the shear wave and thermal wave correspondingly into the liquid. Particles oscillating in the sound wave generate these waves, which damp in the particle vicinity. The characteristic distance for the shear wave amplitude to decay is the "viscous depth" δ_v. The corresponding distance for the thermal wave is the "thermal depth" δ_t. The following expressions give these parameters values in the dilute systems:

$$\delta_v = \sqrt{\frac{2\nu}{\omega}} \tag{9.1}$$

$$\delta_t = \sqrt{\frac{2\tau}{\omega\rho C_p}} \tag{9.2}$$

where ν is the kinematic viscosity, ω is the frequency, ρ is the density, τ is heat conductance, C_p is a heat capacity at constant pressure.

The relationship between δ_v and δ_t has been considered before. For instance, McClements plots "thermal depth" and "viscous depth" versus frequency [4]. It is easy to show that "viscous depth" is 2.6 times more than "thermal depth" in aqueous dispersions [16]. As a result, the particle viscous layers overlap at the lower volume fraction more than the particle thermal layers. Overlap of the boundary layers is the measure of the corresponding particle–particle interaction. There is no particle interaction when corresponding boundary layers are sufficiently separated.

Thus, an increase in the dispersed volume fraction for a given frequency first leads to the overlap of the viscous layers because they extend further into the liquid. Thermal layers overlap at higher volume fractions. This means that the particle hydrodynamic interaction becomes more important at the lower volume fractions than the particle thermodynamic interaction.

The 2.6 times difference between δ_v and δ_t leads to a large difference in the volume fractions corresponding to the beginning of the boundary layers' overlap. The dilute case theory is valid for the volume fractions smaller than these critical volume fractions φ_v and φ_t. These critical volume fractions, φ_v and φ_t, are functions of the frequency and particle size. These parameters are conventionally defined from the condition that the shortest distance between particle surfaces is equal to $2\delta_v$ or $2\delta_t$. This definition gives the following expression for the ratio of the critical volume fractions in aqueous dispersions:

$$\frac{\varphi_v}{\varphi_t} = \left(\frac{a\sqrt{\pi f} + 2.6^{-1}}{a\sqrt{\pi f} + 1}\right)^3 \tag{9.3}$$

where a is particle radius in microns, and f is the frequency in MHz.

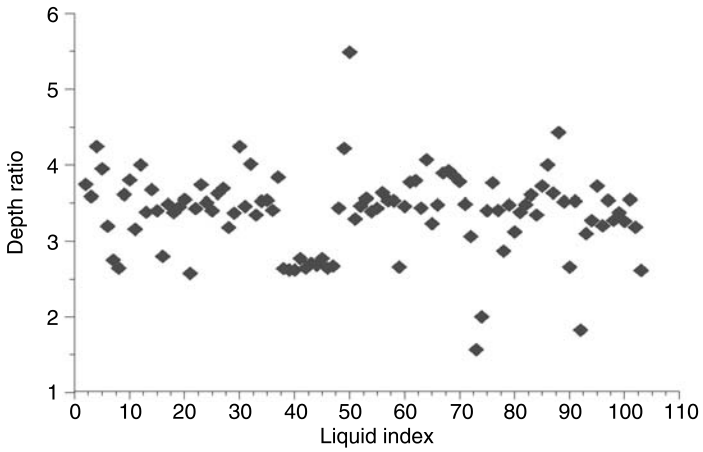

FIGURE 9.1 Ratio of viscous and thermal depth for various liquids.

The ratio of the critical volume fractions depends on the frequency. For instance for neoprene latex, the critical "thermal" volume fraction is 10 times higher than the critical "viscous" volume fraction for 1 MHz and only three times higher for 100 MHz.

It is interesting that this important feature of the "thermal losses" works for almost all liquids. We have more than 100 liquids with their properties in our database. The core of this database is the well-known paper by Anson and Chivers [17]. We can introduce a parameter referred to as "depth ratio":

$$\text{depth ratio} = \frac{\delta_v}{\delta_t}$$

This parameter is 2.6 for water, as mentioned before. Figure 9.1 shows values of this parameter for all liquids from our database relative to the viscous depth of water. It is seen that this parameter is even larger for many liquids.

Therefore "thermal losses" are much less sensitive to the particle–particle interaction than "viscous losses" for almost all known liquids. It makes ECAH theory valid in a much wider range of emulsion volume fractions than one would expect.

There is one more fortunate fact for ECAH theory that follows from the values of the liquid's thermal properties. In general, ECAH theory requires information about three thermodynamic properties: thermal conductivity τ, heat capacity C_p, and thermal expansion β. It turns out that τ and C_p are almost the same for all liquids except water. This reduces the number of required parameters to one – thermal expansion. This parameter plays the same role in "thermal losses" as density in "viscous losses."

ECAH theory has a great disadvantage of being mathematically complex. It cannot be generalized for particle–particle interactions. This is not important as we have found for emulsions, but may be important for latex systems, and is certainly very important for the high density contrast systems. There are two ways to simplify this theory using a restriction on the frequency and particle size. The first is the so-called "long wave requirement" [11] which requires the wave length of the sound wave λ to be larger than particle radius a. This "long wave requirement" restricts particle size for a given set of frequencies. Our experience shows that particle size must

be below 10 microns for the frequency range from 1 to 100 MHz. This restriction is helpful for characterizing small particles.

The long wave requirement provides a sufficient simplification of the theory for implementing particle–particle interaction. Work has been done by Dukhin and Goetz [18] on the basis of the "coupled phase model" [19,20]. This new theory [18] works up to 40% vol even for heavy materials, including rutile.

There is another approach to acoustics, which employs a "short wave requirement" [21]. This approach works only for large particles above 10 microns and requires limited input data about the sample. This theory may provide an important advantage in the case of emulsions and latex systems when the thermal expansion is not known.

There is opportunity in the future to create a mixed theory that could use a polynomial fit merging together "short" and "long" wave range theories. Such combined theory will be able to cover a complete particle size range from nanometers to millimeters for concentrated systems.

There are two recent developments in the theory of acoustics, which deserve to be mentioned here. The first one is a theory of acoustics for flocculated emulsions [22]. It is based on ECAH theory but it uses in addition an "effective medium" approach for calculating thermal properties of the flocs. The success of this idea is related to the feature of the thermal losses that allows for insignificant particle–particle interactions even at high volume fractions. This mechanism of acoustic energy dissipation does not require relative motion of the particle and liquid. Spherical symmetrical oscillation is the major term in these kinds of losses. This provides the opportunity to replace the floc with an imaginary particle assuming a proper choice of the thermal properties.

Another significant recent development is associated with Temkin, who, in his recent papers [23,24], offers a new approach to the acoustic theory. Instead of assuming a model dispersion consisting of spherical particles in a Newtonian liquid, he suggests that the thermodynamic approach be explored as far as possible. This new theory operates with notions of particle velocities and temperature fluctuations. This very promising theory yields some unusual results [23,24]. It has not been yet used, as far as we know, in commercially available instruments.

9.2.2 Theory of Electroacoustics

Whereas acoustic spectroscopy describes the combined effect of the six separate loss mechanisms, electroacoustic spectroscopy, as it is presently formulated, emphasizes only one of these interaction mechanisms, the electrokinetic losses.

In acoustic spectroscopy sound is utilized as both the excitation and the measured variable, and therefore there is but one basic implementation. In contrast, electroacoustic spectroscopy deals with the interaction of electric and acoustic fields and therefore there are two possible implementations. One can apply a sound field and measure the resultant electric current, which is referred to as the colloid vibration current (CVC), or conversely one can apply an electric field and measure the resultant acoustic field, which is referred to as the electronic sonic amplitude (ESA).

First let us consider the measurement of CVC. When the density of the particles ρ_p differs from that of the medium ρ_m, the particles move relative to the medium under the influence of an acoustic wave. This motion causes a displacement of the internal and external parts of the double layer (DL) (see Figure 9.2). This phenomenon is usually referred to as a polarization of the DL [7]. This displacement of opposite charges gives rise to a dipole moment. The superposition of the electric fields of these induced dipole moments over the collection of particles gives rise to a macroscopic electric field, which is referred to as the colloid vibration potential (CVP). This potential in turn creates electric current, the CVC. Thus, the fourth mechanism of particle interaction with sound leads to the transformation of part of the acoustic energy to the

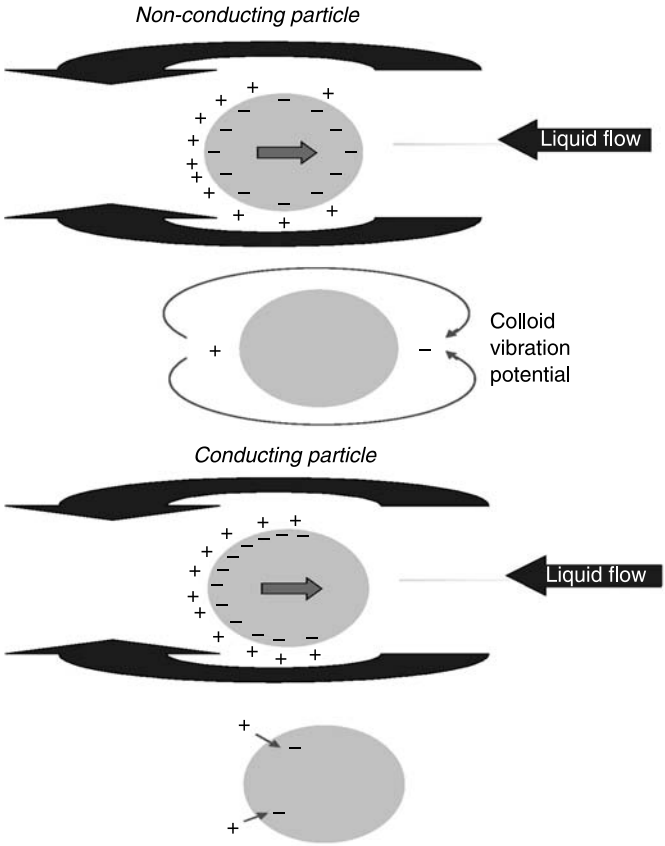

FIGURE 9.2 Illustration of the exterior DL polarization by the liquid flow relative to the particle surface induced with ultrasound.

electric energy. This electric energy may then be dissipated if the opportunity exists for the flow of electric current.

Now let us consider the measurement of ESA, which occurs when an alternating electric field is applied to the disperse system [9]. If the zeta potential of the particle is greater than zero, then the oscillating electrophoretic motion of the charged dispersed particles generates a sound wave.

Both electroacoustic parameters, CVC and ESA, can be experimentally measured. The CVC or ESA spectrum is the experimental output from electroacoustic spectroscopy. Both of these spectra contain information about zeta potential and PSD. However, only one of the electroacoustic spectra is required because both of them contain essentially the same information about the dispersed system.

The conversion electroacoustic spectra into the PSD requires theoretical model of the electroacoustic phenomena. This conversion procedure is much more complicated for electroacoustics comparing to the acoustics. The reason for the additional problems relates to the additional field involved in the characterization: electric field. The theory becomes much more complicated because of this additional field.

For some time O'Brien's theory [25,26] has been considered as a basis for electroacoustics. It provides a widely accepted expression for the dynamic electrophoretic mobility μ_d (Equation 5.28

in Ref. 4); that is:

$$\mu_d = \frac{2\varepsilon_0\varepsilon_m\varsigma(\rho_p - \rho_s)\rho_m}{3\eta(\rho_p - \rho_m)\rho_s} G(s,\varphi)(1 + F(Du,\omega',\varphi)) \tag{9.4}$$

where ε_0 and ε_m are dielectric permittivities of the vacuum and liquid, ζ is the electrokinetic potential, η is dynamic viscosity, ρ_m, ρ_p, and ρ_s are the densities of liquid, particle, and dispersion, $\omega' = \frac{\omega}{\omega_{MW}}$, $\omega_{MW} = \frac{K_m}{\varepsilon_0\varepsilon_m}$, K_m is conductivity of the media, ω is frequency of ultrasound, and $Du = \kappa^\sigma / K_m a$ is the Dukhin number that reflects the contribution of the surface conductivity κ^σ.

Function G presents the contribution of hydrodynamic effects, whereas function F reflects electrodynamic aspects of the electroacoustic phenomena.

This initial theory by O'Brien does not take into account hydrodynamic and electrodynamic interactions. Later, two more theories were developed for oil-in-water emulsions. The first, by O'Brien, is presented in a review, Ref. 9. The second is by Dukhin et al. (see Refs. 27–29, and Chapter 5 in Ref. 6).

Application of these theories to water-in-oil emulsions is complicated by the conductivity of the water droplets. In order to apply this theory to water-in-oil emulsions we should simply introduce the conductivity of the particles in the expression for function F. A water-in-oil emulsion can be considered as conducting particles in a non-conducting media. In order to achieve this we should simply use a more general expression for the Dukhin number:

$$Du = \frac{K_p}{K_m} + \frac{\kappa^\sigma}{K_m} \tag{9.5}$$

where K_p is conductivity of water droplets.

This modified Dukhin number can be used in the general expression for the F function:

$$F(Du,\omega',\varphi) = \frac{(1 - 2Du)(1-\varphi) + j\,\omega'(1 - \frac{\varepsilon_p}{\varepsilon_m})(1-\varphi)}{2(1 + Du + \varphi(0.5 - Du)) + j\omega'(2 + \frac{\varepsilon_p}{\varepsilon_m} + \varphi(1 - \frac{\varepsilon_p}{\varepsilon_m}))} \tag{9.6}$$

The properties of the water-in-oil emulsion allow us to approximate the value of this function. It is known that the conductivity of water is much higher than the conductivity of nonpolar liquids. This means that

$$Du \approx \frac{K_p}{K_m} \gg 1 \tag{9.7}$$

In addition, the dielectric permittivity of water is about 40 times higher than the permittivity of nonpolar liquids:

$$\frac{\varepsilon_p}{\varepsilon_m} \gg 1 \tag{9.8}$$

Using these two strong inequalities we can neglect 1 in comparison to the relevant parameters in Equation 9.3. As a result we obtain the following approximate value for the function F in

water-in-oil emulsions:

$$F(Du, \omega', \varphi) \approx \frac{1-\varphi}{1-\varphi} \frac{-2Du - j\,\omega' \dfrac{\varepsilon_p}{\varepsilon_m}}{2Du + j\omega' \dfrac{\varepsilon_p}{\varepsilon_m}} = -1 \tag{9.9}$$

This approximate value is actually quite accurate due to the large conductivity and permittivity of water.

If we use this value for function F in Equation 9.4 for the dynamic mobility, we would come to the interesting result:

$$\mu_d \left(\frac{K_p}{K_m} \gg 1, \frac{\varepsilon_p}{\varepsilon_m} \gg 1 \right) = 0 \tag{9.10}$$

for thin isolated DLs only.

This means simply that water-in-oil emulsions with isolated and thin DLs should not exhibit any electroacoustic effect.

It is possible to give a simple explanation to this unexpected conclusion. In order to do this we compare the electric field structure induced by the relative particle–liquid motion for non-conducting and conducting particles, as illustrated in Figure 9.2.

It is known that ultrasound generates particle motion relative to the liquid due to the density contrast. In drawing Figure 9.2 we assume that the particles move from left to right. This causes a liquid motion, relative to the particle surface, which is illustrated with arrows above and below the particle.

This motion of the liquid drags ions within the diffuse layer towards the left pole of the particle. This redistribution of the diffuse layer leads to the different results for conducting and non-conducting particle.

In the case of non-conducting particle, the surface charge cannot move. It retains its spherical symmetry. As a result the particle gains an excess negative charge at the right hand side pole and excessive positive charge at the left hand side pole. It gains a dipole moment. This dipole moment generates an external electric field, which gives rise to the colloid vibration current.

In the case of a conducting particle, the charge carriers inside the particle can follow the counter-ions of the DL that are being dragged to the left hand side pole. This means that the surface charge, or charge associated with the particle, loses its internal spherical symmetry as well as the charge of the diffuse layer. Most importantly, each element of the surface, as well as the adjacent diffuse layer, remains electroneutral. No external electric field appears and electroacoustic effect is practically zero.

This does not mean that electroacoustics is useless for water-in-oil emulsions. It is known that existing electroacoustic theories for both ESA and CVC effects do not take account of overlapping of the double layers (DLs). There is only one exception, the recently created Shilov's theory [30].

The assumption of isolated, not-overlapped, double layers requires either a large droplet radius a or a sufficiently high ionic strength leading to a shorter Debye length κ^{-1}. Figure 9.3 illustrates approximately the range of volume fractions φ, where assumption of isolated DLs is valid for given κa, following Ref. 6. It is seen that water-in-oil emulsions should have overlapped DLs at very low volume fractions due to the large κ^{-1}. In the water-in-oil emulsions with overlapped DLs the nature of electroacoustic effect is quite different.

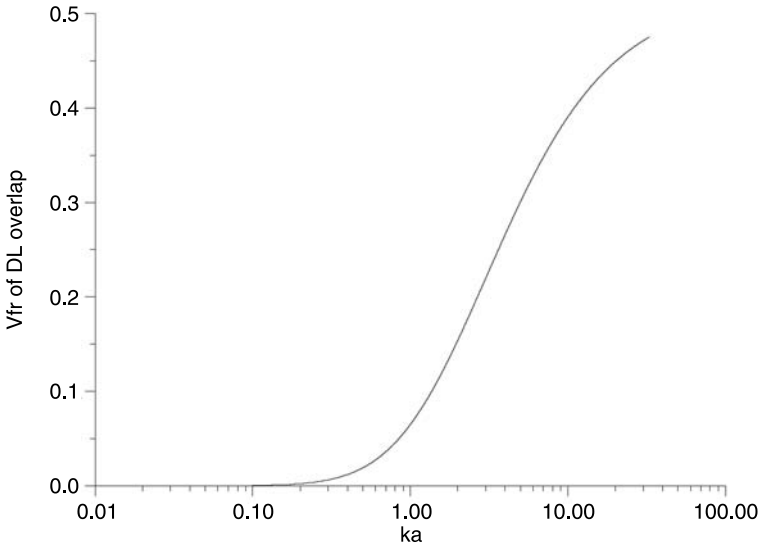

FIGURE 9.3 Estimate of the volume fraction of the overlap of the electric double layer.

Homogeneous distribution of the counter-ions eliminates polarization charges induced on the left hand side pole of the particles by the liquid motion. The electroacoustic effect is related simply to the displacement current of the oscillating motion of the particle surface charges. Shilov's theory [30] describes this effect. It yields the following expression for the dynamic mobility:

$$\mu_d = \frac{2\sigma a}{3} \frac{\rho_m}{\rho_s \eta \Omega + i\omega (1-\varphi) \dfrac{2a^2}{9} \rho_p \rho_m} \tag{9.11}$$

where σ is surface charge density, Ω is a hydrodynamic drag coefficient, and ω is the ultrasound frequency.

It is seen that there are no electrodynamic parameters for either the particles or the media involved in this expression. This leads us to the conclusion that, in the case of overlapped DLs, water-in-oil emulsions generate an electroacoustic signal in a similar manner as non-conducting particles.

According to Shilov's theory, in the case of overlapped DLs, we can calculate the surface charge of the particles from the dynamic mobility knowing nothing about the relevant ions or even the ionic strength. We know of only one other electrokinetic theory with a similar level of simplicity – Smoluchowski's theory.

This general nature of Shilov's theory is especially important for nonpolar liquids. The calculation of zeta potential requires information on the ions, because it includes Debye length

$$\sigma = \frac{1}{3} \frac{RT}{F} \frac{1-\varphi}{\varphi} \varepsilon_0 \varepsilon_m a \kappa^2 \sinh \frac{F\zeta}{RT} \tag{9.12}$$

where T is absolute temperature, F is Faraday constant, and R is a gas constant. This simple analysis leads to the following conclusions:

1. A water-in-oil emulsion with isolated DLs should not generate any electroacoustic signal
2. A measurable electroacoustic signal generated by water-in-oil emulsion indicates that DLs are overlapped

9.3 GENERAL FEATURES OF ACOUSTIC MEASUREMENT

In this section we present some requirements of the acoustic measurement that we could derive from our experience dealing with ultrasound-based characterization techniques.

9.3.1 Attenuation or Sound Speed?

As mentioned previously, there are two measurable acoustic parameters: attenuation and sound speed. The question arises as to which one is better for characterizing a particular effect in a given food product. There are two answers to this question in the general scientific literature. For example, J. McClements, a very well known scientist in the field of ultrasound characterization of food products, stresses the importance of the sound speed [12,13]. In contrast, our group at Dispersion Technology Inc. relies mostly on attenuation. It is clear that this question deserves special consideration.

We have performed several simple tests for answering this question. First, we have measured sound speed of water varying concentration of several simple chemicals. It turns out that sound speed is very sensitive to the chemical composition (Figure 9.4). It changes roughly 100 m/sec per 1 mol/l of the simple salt. Keeping in mind that precision of the sound speed measurement is roughly 1 cm/sec, we could conclude that it is possible to monitor variation of the water chemical composition with precision of 0.0001 mol/l. Sound speed is also very sensitive to the temperature. For water it changes 2.4 m/sec per degree Celsius.

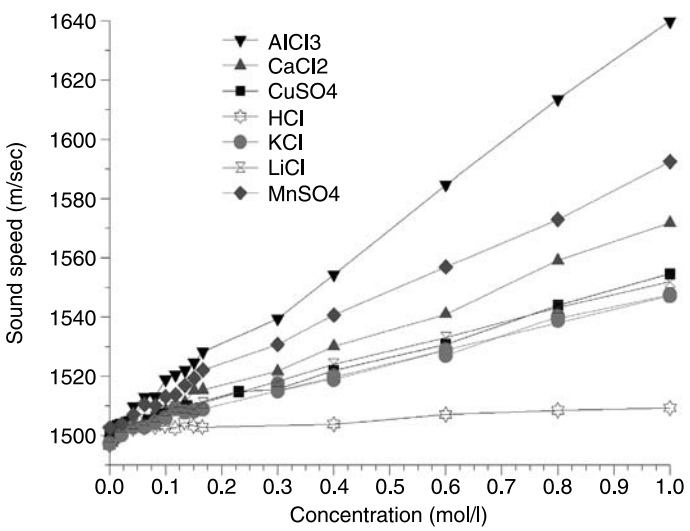

FIGURE 9.4 Sound speed of water versus concentration of various simple chemicals.

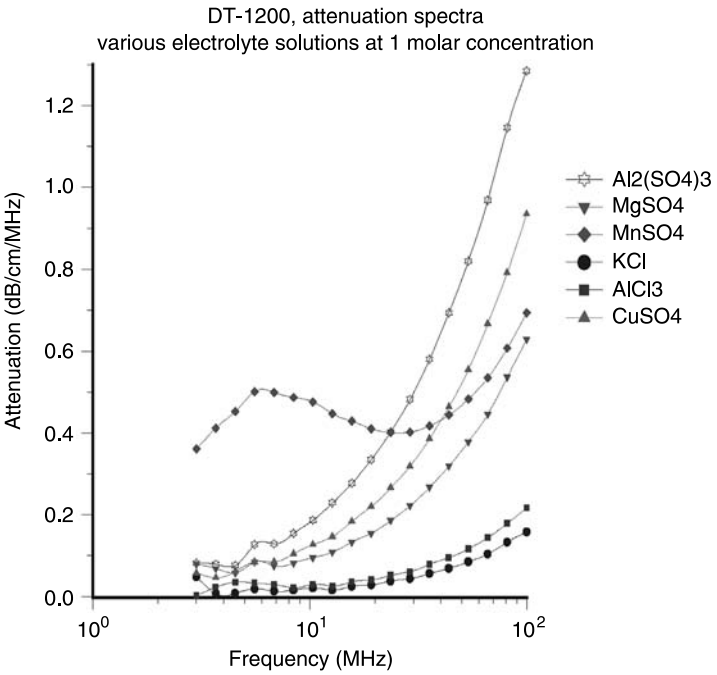

FIGURE 9.5 Attenuation of water versus concentration of various simple chemicals.

Attenuation in turn is much less sensitive to chemical composition. Figure 9.5 shows attenuation spectra of water at 1 mol/l concentration of similar chemical additives. It is seen that even at this very high concentration it changes significantly only for rather charged ions. This influence is much less pronounced at lower concentration, which we could expect in food products. Figure 9.6 shows that even for 2:2 valency salt it changes 0.1 dB/cm/MHz only at 0.14 mol/l. It might be generally concluded that the impact of chemical variation on attenuation is negligible if concentration varies less than 0.1 mol/l.

Attenuation is not very sensitive to the molecular and ionic composition, but it changes dramatically with composition of the dispersed phase. In other words, attenuation reflects variation occurring on the scale of colloid sizes, from nanometers to microns, whereas sound speed is more representative for effects that originate on the molecular scale of angstroms.

This simple analysis indicates that sound speed is the better parameter for investigating effects on the molecular scale, whereas attenuation is more suitable for characterizing effects related to the heterogeneity and phase composition of the particular system.

9.3.2 Ranges of Values

The next point of interest is the potential range of attenuation and sound speed in food products. Sound speed varies within the range 1000–2000 m/sec for practically all food products. For water-based food products it would be close to 1500 m/sec, which is sound speed of water at room temperature.

Attenuation varies in much wider dynamic range. That is why it is normally expressed on a logarithmic scale in decibels (dB).

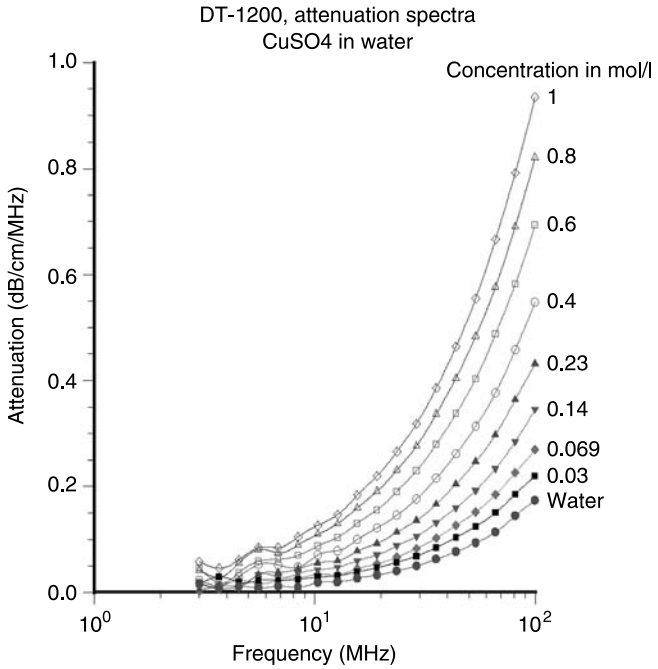

FIGURE 9.6 Attenuation of water versus concentration of $CuSO_4$.

Water is the least attenuating liquid. Its attenuation expressed in units of dB/cm/MHz increases linearly with frequency reaching 0.2 at 100 MHz.

According to our experience, an acoustic spectrometer must be able to cover a dynamic range from water up to 20 dB/cm/MHz for a complete frequency range from 1 to at least 100 MHz.

9.3.3 Precision

It is also possible to derive some conclusions regarding precision of the acoustic measurement because it depends directly on the precision of monitoring and maintaining other parameters.

For instance, it is practically impossible to maintain a uniform temperature of the sample and instrument with variations less than 0.01 °C. We know that a variation in temperature of 1 °C leads to the sound speed variation of water 2.4 m/sec. Following this number, a variation of 0.01 °C corresponds to the variation of sound speed of about 1 cm/sec. This is about 10^{-5} of the absolute sound speed.

Higher precision of the sound speed measurement makes no sense because uncontrolled temperature variations would mask it.

It is possible to make a similar estimate of the sound speed measurement precision using chemical composition variations. It is known that maintaining dissolved ion and molecule composition in water with precision higher than 10^{-4} mol/l is practically impossible. Adsorption of various chemical species from the atmosphere would create larger uncontrolled variations. Figure 9.4 indicates that sound speed changes about 100 m/sec per mol/l of the simple salts. This leads us to the sound speed precision of 1 cm/sec for the smallest controllable variations of

the chemical composition. It is interesting that this level of precision is practically identical to the one calculated from the temperature stability requirement.

Unfortunately, it is impossible to estimate precision of attenuation measurement using similar analysis. As we mentioned above, attenuation is much less sensitive to variations in chemical composition and temperature. Attenuation depends mostly on the composition and state of the dispersed phase, particles, and droplets. As a result precision of its measurement must be related somehow to the particles.

We have done this using resolution of the attenuation measurement for characterizing content of the large particles (see Chapter 8 in Ref. 6). It turns out that in order to resolve a single 1 micron particle on the background of the 100,000 particles with size 100 nm, attenuation must be measured with precision of 0.01 dB/cm/MHz.

9.3.4 Frequency Range

The frequency range might be different depending on the purpose of the measurement. For droplet size distribution, the wider the frequency range, the more information about the system can be extracted. It turns out that measurement within frequency range from 1 to 100 MHz makes it possible to characterize sizes as small as 5 nm, as it will be shown with water-in-heptane microemulsion. Restricting the frequency range to the lower frequencies would limit dramatically the small size limit. It would also restrict the ability to characterize details of the particle size distribution. The frequency range specified above makes it possible to characterize bimodality, which would be impossible if high frequencies are not included in the measurement.

At the same time, low frequency attenuation below 10 MHz could be affected by bubbles. This is especially important for process control, when consistent removal of bubbles might present a problem.

This factor might be especially important for fat content measurement. It requires just one frequency, which simplifies electronics and software. Position of this frequency is open for discussion. From the cost viewpoint it is highly desirable to make this frequency as low as possible. This would reduce transducer and electronics costs. However, low frequency attenuation is highly affected by bubbles. In addition, low frequency attenuation is very sensitive to the droplet size. Elimination or at least minimization of these two factors (bubbles and droplet size) would require frequency above 10 MHz. Frequency in the range 40–50 MHz might be optimal.

9.4 APPLICATIONS

There are many instances of successful characterization of the particle size distribution and zeta potential of emulsion droplets. There are two quite representative reviews of these experiments published by McClements [4] (acoustics) and Hunter [9] (electroacoustics). We present here some more recent results that have not been published in any reviews.

9.4.1 Dairy Products: Droplet Sizing

We use dairy products from two different sources. The first is a local A&P supermarket. We purchased various milks and butters. Containers of these products present table of product composition, including fat, proteins, and sugar content. We use some of these data in our analysis. In addition we have two samples of the whole milk supplied by the Department of Food Science at Cornell University (courtesy of Dr Carmen Moraru). One of the samples is homogenized, whereas the other is unhomogenized. These samples have well defined compositions: 3.9%

fat, 3.25% proteins, and 4.6% lactose. These two samples allow us to verify the particle size calculation procedure.

There is no special sample preparation involved. Milks and butters are measured "as is," with no dilution. Milk is simply poured into the DT-100 sample chamber with a volume between 20 ml and 100 ml depending on the instrument setup. There is no mixing or pumping applied for measuring attenuation of the stable products. DT-100 has a built-in magnetic stirrer, which can be used for mixing unstable samples. It is used for measuring sound speed during milk spoiling processes.

Butter is pushed into the chamber at the temperature around 25 °C when it becomes a soft gel-like substance. Measurement must be performed when the gap between the transducer and receiver closes. It is opposite to the normal mode of DT-1200 functioning.

We use unsalted butter for extracting pure milk fat. This is necessary for measuring the intrinsic acoustic properties of the fat. Heating the butter leads eventually to its phase separation. We use a middle phase that is supposed to be a pure milk fat with no water, proteins, or other constituents.

Attenuation frequency spectra could be considered as experimental data. Figure 9.7 presents attenuation spectra for general dairy products. The legends on this figure indicate the type of the dairy product, relative fat content according to the manufacturer label, date and time of the measurement. This figure shows only one curve for each product. Actually, each product is measured several times for controlling reproducibility. Figure 9.8 shows multiple measurements for the low fat products.

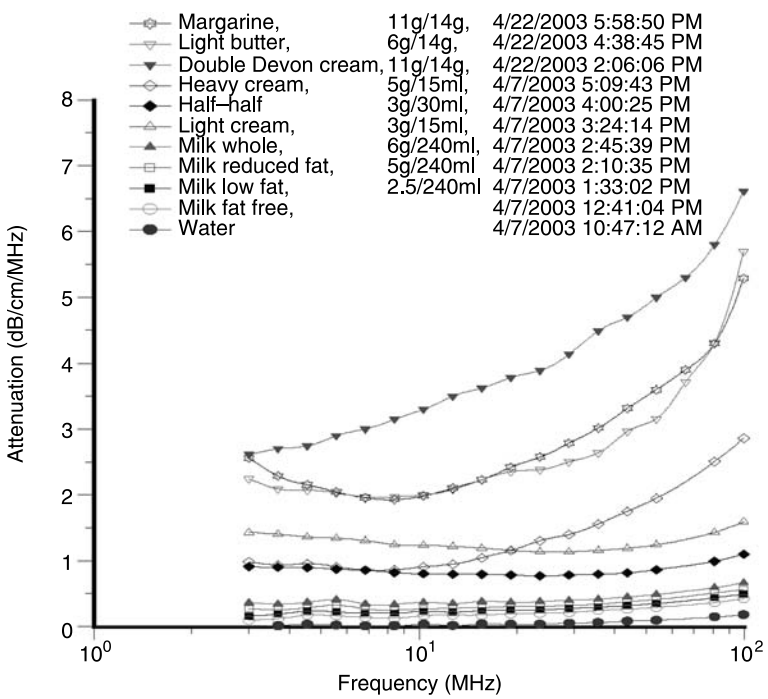

FIGURE 9.7 Attenuation of various dairy products.

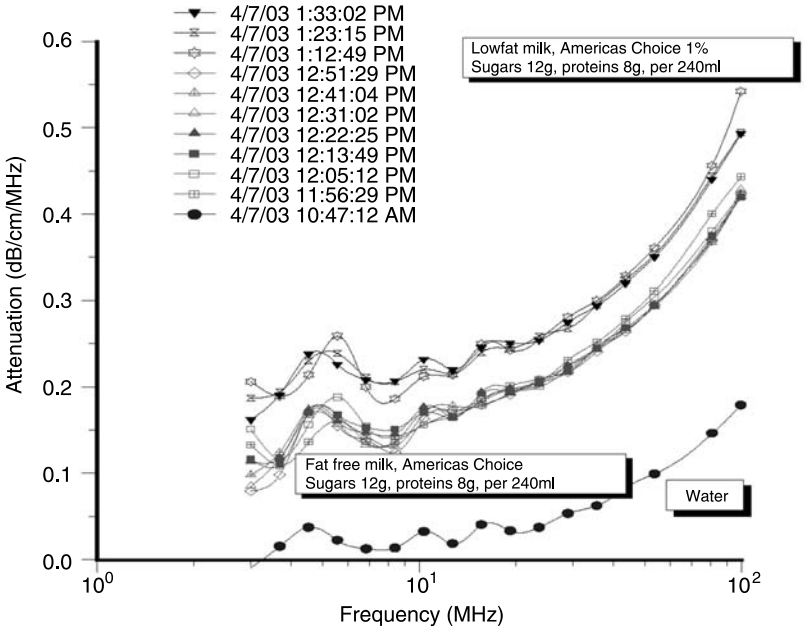

FIGURE 9.8 Precision test with low fat content milks.

Figure 9.9 provides attenuation spectra for the samples from Cornell University. These samples are identical in composition but different in terms of water droplet size distributions. A distinctive difference in attenuation spectra of these samples is a clear proof that acoustic spectroscopy can be used for particle sizing in dairy systems. Attenuation spectra within frequency range from 3 to 100 MHz contain information on the droplet size distribution. We show below how this information could be extracted.

Calculation of the droplet size distribution and fat content requires certain information on the milk fat properties. That is why we measured attenuation spectra of the pure milk fat. It is shown in Figure 9.10. It turns out that acoustic properties of the milk fat are very temperature dependent. In order to incorporate this temperature dependence into the size calculation we measured dependence of the fat attenuation on the temperature. It is almost linear, as shown in Figure 9.11.

Experimental data contains information for calculating droplet size distribution and/or fat content of these samples. Calculation of the droplet size distribution requires some input parameters for each phase. This set of the input parameters depends strongly on the properties of the system.

Dairy products are emulsions, oil-in-water for milks and water-in-oil for butters. The densities of fat and water are very close. This eliminates a viscous dissipation mechanism of the ultrasound attenuation. In addition, droplet size of these systems usually does not exceed 10 microns. In combination with the low density contrast this practically eliminates scattering effect.

This simple analysis leads to the conclusion that ultrasound attenuation in the dairy products occurs mostly due to the thermal dissipation and intrinsic attenuation of the water and fat phases. We can describe these systems as "soft particles" using terminology from Ref. 6. Therefore, we need a set of thermodynamic properties for each phase, such as thermal conductivity τ (J/m sec K), heat capacity C_p (J/kg K), and thermal expansion β (10^{-4} K^{-1}). In addition

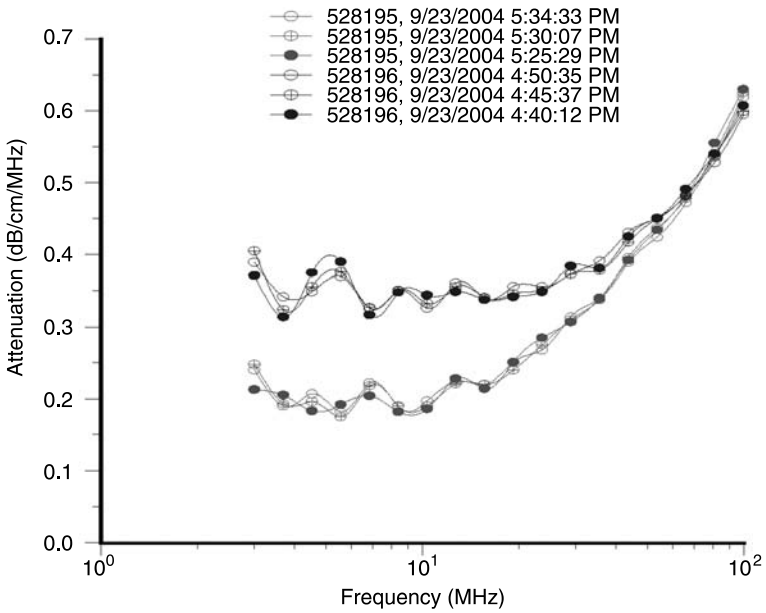

FIGURE 9.9 Attenuation spectra of the whole milk and homogenized milk.

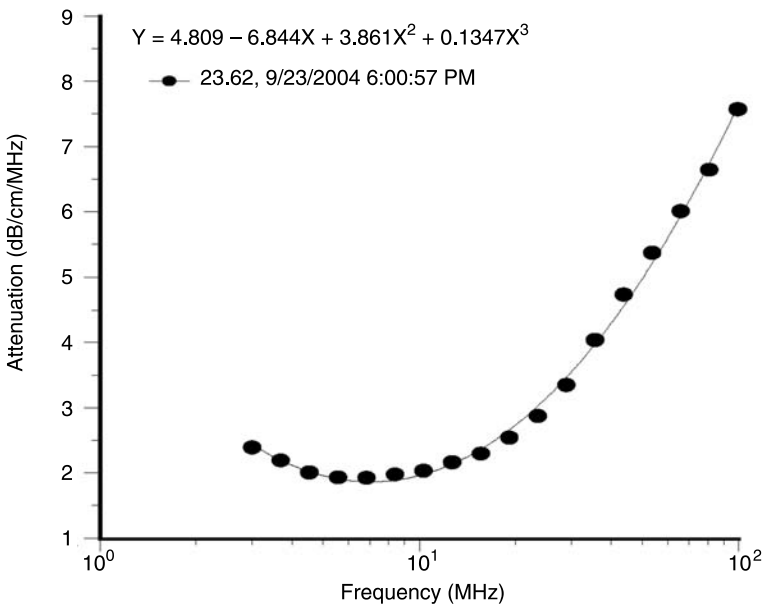

FIGURE 9.10 Intrinsic attenuation of the milk fat at room temperature.

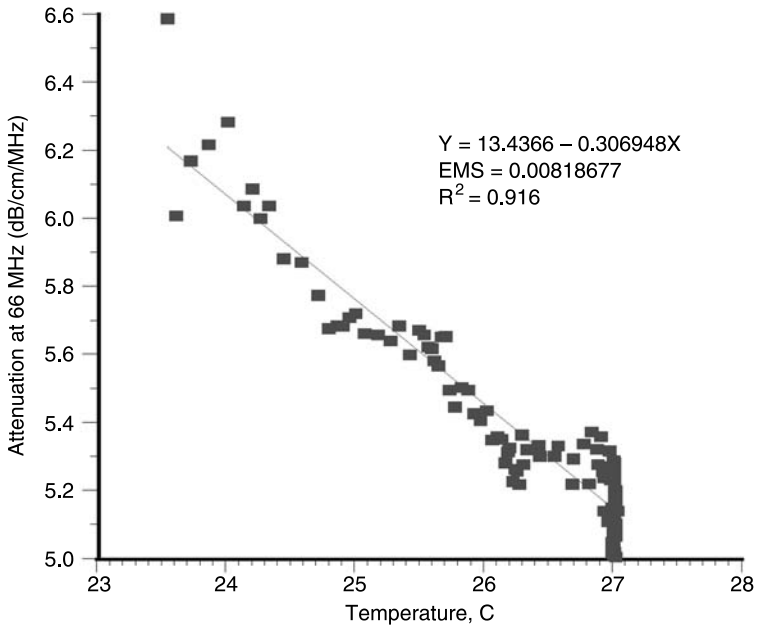

FIGURE 9.11 Temperature dependence of the milk fat attenuation at 66 MHz.

TABLE 9.1
Thermodynamic Properties of the Milk Fat and Water Phase Around Room Temperature

	Thermal conductivity (J/m s K)	Heat capacity (J/kg K)	Thermal expansion (10^{-4} K^{-1})	Attenuation (dB/cm/MHz) – frequency (MHz) function
Water	0.61	4.18	2.07	$\alpha = 4.809 - 6.844\omega + 3.861\omega^2 + 0.147\omega^3$
Milk fat	0.17	2.1 (at 40 °C)	6.2	$\alpha = 0.002\omega$

we need the intrinsic attenuation of the fat and water phases. Attenuation of the fat might be frequency (ω) dependent. That is why we should specify a function $\alpha(\omega)$ that describes this dependence. Thermodynamic properties and intrinsic attenuation of the milk fat and water are summarized in Table 9.1.

It is important to mention here that we neglect for the time being influence of proteins, sugar, and other additives on the properties of the water phase. This assumption must be verified later. We also neglect temperature dependence of all of these parameters. These two assumptions would create some uncertainty in the calculated droplet size distribution.

Milk is an obvious candidate for verifying particle sizing capability of ultrasound-based techniques. It is known that homogenization leads to substantial reduction of the fat droplet size. Attenuation spectra presented in Figure 9.9 reflects this change. Figure 9.12 shows droplet size distributions calculated from these attenuation spectra using input parameters presented in Table 9.1.

It is interesting to compare contributions of the different mechanisms to the ultrasound attenuation. Figure 9.13 shows these contributions calculated for the size distributions from Figure 9.12.

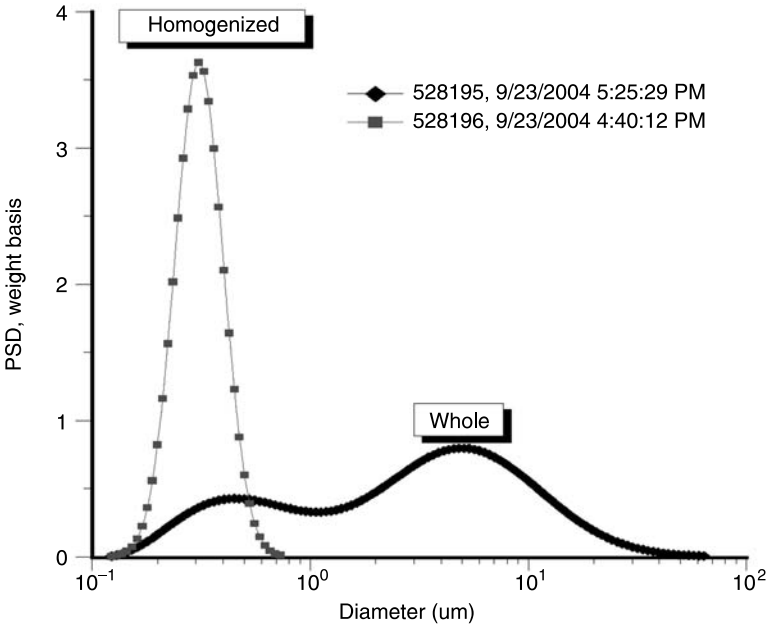

FIGURE 9.12 Droplet size distributions of the fat in whole and homogenized milks.

It is seen that at low frequency thermal attenuation and intrinsic attenuation are comparable. At the high frequency intrinsic attenuation dominates. This conclusion would have a profound effect for fat content calculation. At this point we could conclude that low frequency range below 10 MHz is the most important for particle sizing.

The more interesting feature of acoustic attenuation characterization procedure is that it allows characterization of droplet size distribution even in gel like systems, like butter, with no dilution or melting. It is possible because thermal attenuation effect is thermodynamic in nature; it does not require relative droplet–liquid motion.

Figure 9.14 shows size of the water droplets in light butter. The second graph on Figure 9.14 presents theoretical attenuations with intrinsic and thermal contributions. Intrinsic contribution is much higher in this case because it corresponds to the pure fat, not to the water. It dominates high frequency spectra even more than in the case of milks.

These calculations use the same thermodynamic properties of the fat as in the case of the milks.

9.4.2 Dairy Products: Fat Content

Fat content is a very important quality control parameter of the dairy products. Attenuation measurement offers a simple way to characterize it with no special treatment of the sample. Figure 9.7 shows attenuation spectra of the various dairy products. It is clear that attenuation increases with increasing fat content. This dependence could be used for calculating fat content.

In previous sections we showed that total ultrasound attenuation consists of thermal dissipation and intrinsic attenuation. Thermal dissipation is droplet size dependent, whereas intrinsic attenuation is not sensitive to the variation of the droplet size.

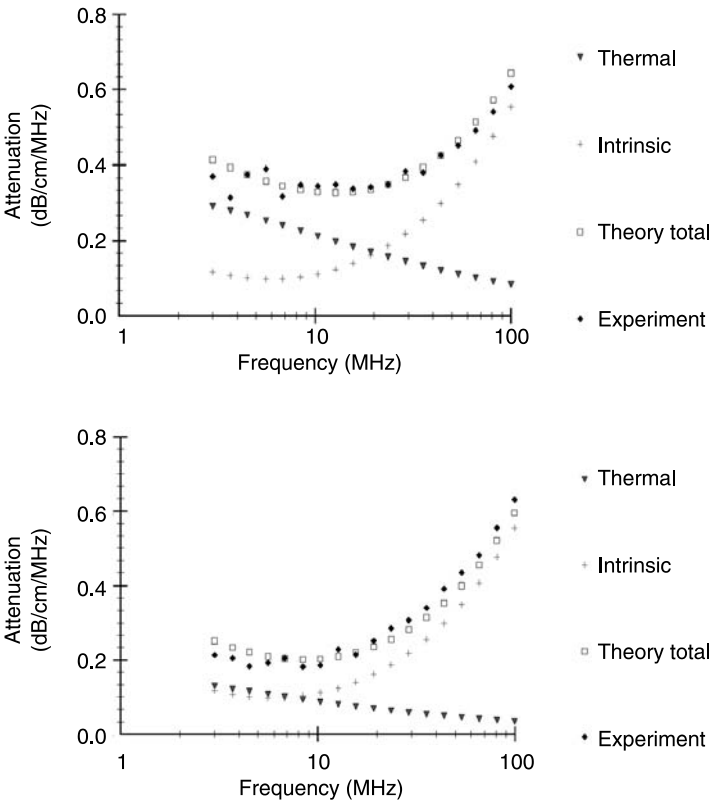

FIGURE 9.13 Experimental and theoretical attenuations for whole milk and homogenized milk.

Dependence on the droplet size would complicate characterization of the fat content. In order to minimize this factor we should use attenuation at the frequency range where intrinsic effect dominates. Figures 9.13 and 9.14 indicate that it is high frequency range, above at least 40 MHz.

Figure 9.15 shows attenuation at 44 MHz plotted versus fat weight fraction. We use data from Figure 9.7 for generating this graph. It is seen that there is practically linear correlation between attenuation and fat content. This might be used as a simple and direct way of determining this parameter.

We might expect a high reproducibility of this procedure because attenuation spectra measured for different brands of the same dairy product are practically the same. Figure 9.16 shows this for two different half–half milks.

9.4.3 Microemulsion

The mixture of heptane with water and AOT is a classic three components system. It has been widely studied due to a number of interesting features it exhibits. This system forms stable reverse microemulsions (water-in-oil) without the complication introduced by additional cosurfactant. Such a cosurfactant (usually alcohol) is required by many other reverse microemulsion systems. This simplification makes the alkane/water/AOT system a model for studying reverse microemulsions.

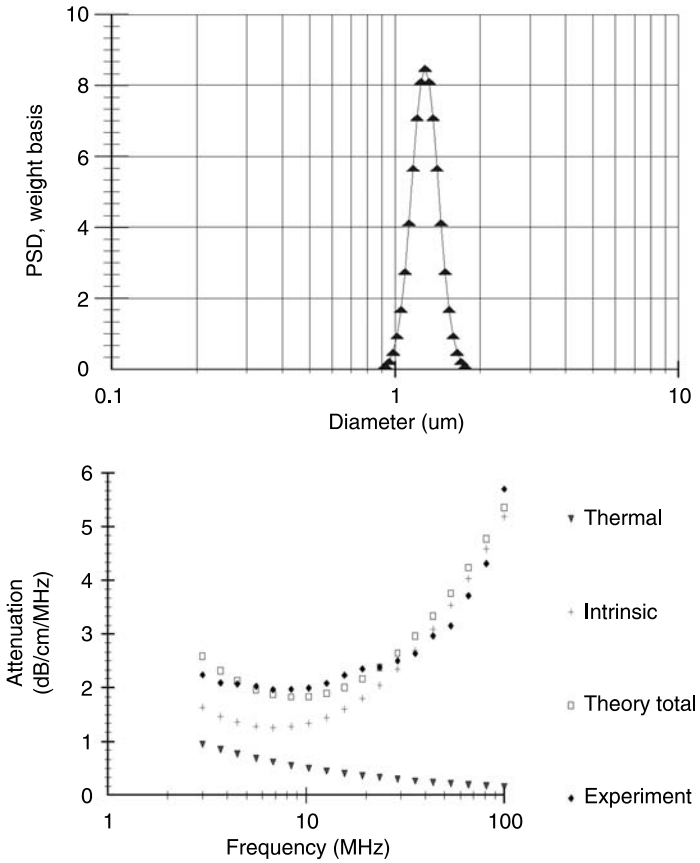

FIGURE 9.14 Droplet size distribution of the water droplets in light butter and corresponding attenuation spectra.

There have been many studies devoted to characterization of these practically important systems. Reverse emulsion droplets have been used as chemical micro reactors to produce nano size inorganic and polymer particles with special properties that are not found in the bulk form. These microemulsion systems have also been a topic of research for biological systems and the AOT head groups have been found to influence the conformation of proteins and increase enzyme activity. The unique environment created in the small water pools of swollen reverse micelles allows for increased chemical reactivity. The increase in surface area with decrease in size of the droplets also can significantly increase reactivity by allowing greater contact of immiscible reactants.

There have been many attempts to measure the droplet size of this microemulsion. Several different techniques were used: PCS [28–33], classic light scattering [30,31,34], SANS [35–37], SAXS [29,38,39], ultra-centrifugation [32,34,40], and viscosity [29,32,34]. It was observed that the heptane/water/AOT microemulsions have water pools with diameters ranging from 2 to 30 nm. The water drops are encapsulated by the AOT surfactant so that virtually all of the AOT is located at the interface shell. The size of the water droplets can be conveniently altered by

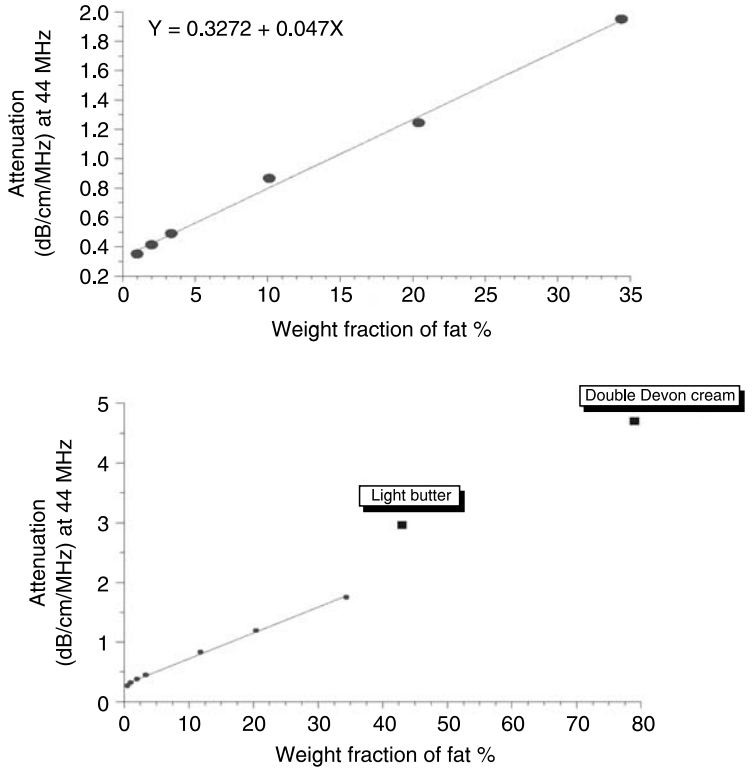

FIGURE 9.15 Attenuation of the oil-in-water dairy products at the single frequency of 44 MHz versus fat content.

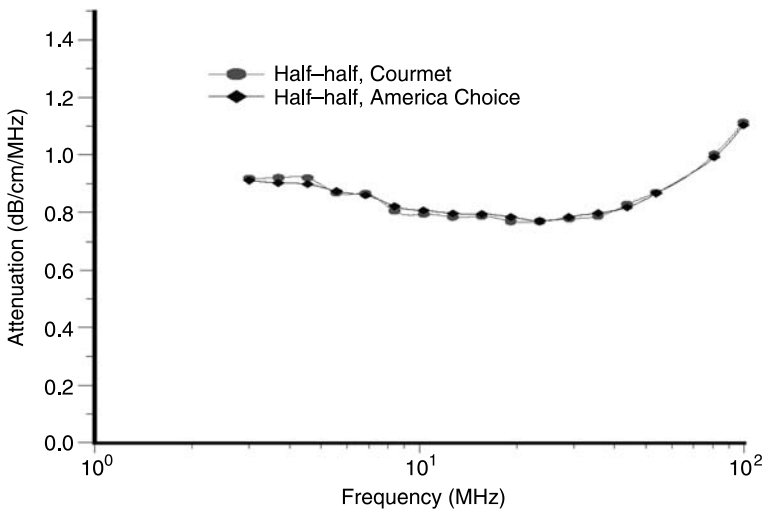

FIGURE 9.16 Attenuation of the half–half milk from different brands.

adjusting the molar ratios of water to surfactant, designated as R ($[H_2O]/[AOT]$). At low R values ($R \leq 10$) the water is strongly bound to the AOT surfactant polar head groups and exhibits unique characteristics different from bulk water. At higher water ratios ($R > 20$) free water is predominant in the swollen reverse micellular solutions, and at approximately $R = 60$, the system undergoes a transition from a transparent microemulsion into an unstable turbid macroemulsion. This macroemulsion separates on standing into a clear upper phase and a turbid lower phase.

The increase in droplet size and phase boundary can also be achieved by raising the temperature up to a critical temperature of 55 °C. In addition this system has been found to exhibit an electrical percolation threshold whereby the conductivity increases by several orders of magnitude by either varying the R ratio or increasing the temperature [37,38,41,42]. Despite all these efforts, there still remain questions regarding the polydispersity of the water droplets, and few studies are available above the R value of 60 where a turbid macroemulsion state exists.

Acoustic spectroscopy offers a new opportunity for characterizing these complicated systems. Details of this experiment are presented in Ref. 43. The reverse microemulsions were prepared by first making a 0.1 molar AOT in heptane solution (6.1% wt. AOT). The heptane was obtained from Sigma as HPLC grade (> 99% purity). Known amounts of 18 MΩ cm water were added to the AOT–heptane solution using a 1 ml total volume, graduated glass syringe, and then shaken for 30 sec in Teflon capped glass bottles. The shaking action was required to overcome an energy barrier to distribute the water into the nano-sized droplets, as it could not be achieved using a magnetic stirrer.

In all cases, the reported R values are based on the added water, and were not corrected for any residual water that may have been in the dried AOT or heptane solvent. Karl Fischer analysis of the AOT–heptane solutions before the addition of water resulted in a R value of 0.4. This amount was considered to be negligible.

Measurements were made starting with the pure water and heptane and then the AOT–heptane sample with no added water ($R = 0$). The sample fluid was removed from the instrument cell and placed in a glass bottle with a Teflon cap. Additional water was titrated and the microemulsion was shaken for 30 sec before being placed back into the instrument cell. The sample cell contained a cover to prevent evaporation of the solvents. The samples were visually inspected for clarity and rheological properties for each R value. These steps were repeated for increasing water weight fraction or R ratios up to $R = 100$. At $R \geq 60$ the microemulsions became turbid. At $R > 80$, the emulsions became distinctly more viscous.

The weight fractions of the dispersed phase were calculated for water only without including the AOT. Each trial run lasted approximately 5 to 10 min with the temperature varied from 25 to 27 °C. A separate microemulsion sample for $R = 40$ was made up a few days prior to the first study. For the $R = 70$ sample, a second acoustic measurement was made with the same sample used for the first study. The complete set of experiments for water, heptane, and the reverse microemulsions from $R = 0$ to 100 was repeated to evaluate the reproducibility.

Attenuation spectra measured in the first run up to $R = 80$ are presented in Figure 9.17. The results for $R = 90$ and $R = 100$ are not reported because they were found to vary appreciably. As the water concentration is increased, the attenuation spectrum rises in intensity and there is a distinct jump in the attenuation spectrum from $R = 50$ to $R = 60$ in the low frequency range. This discontinuity is also reflected in the visual appearance as at $R = 60$ the system becomes turbid. The smooth shape of the attenuation curve also changes at $R > 60$. The stability and reproducibility of the system was questioned due to the irregular nature of the curve so the experiment at $R = 70$ was repeated and gave almost identical results. An additional experiment was run at $R = 40$ for a separate microemulsion prepared a few days earlier. This showed excellent agreement with the results for freshly titrated microemulsion.

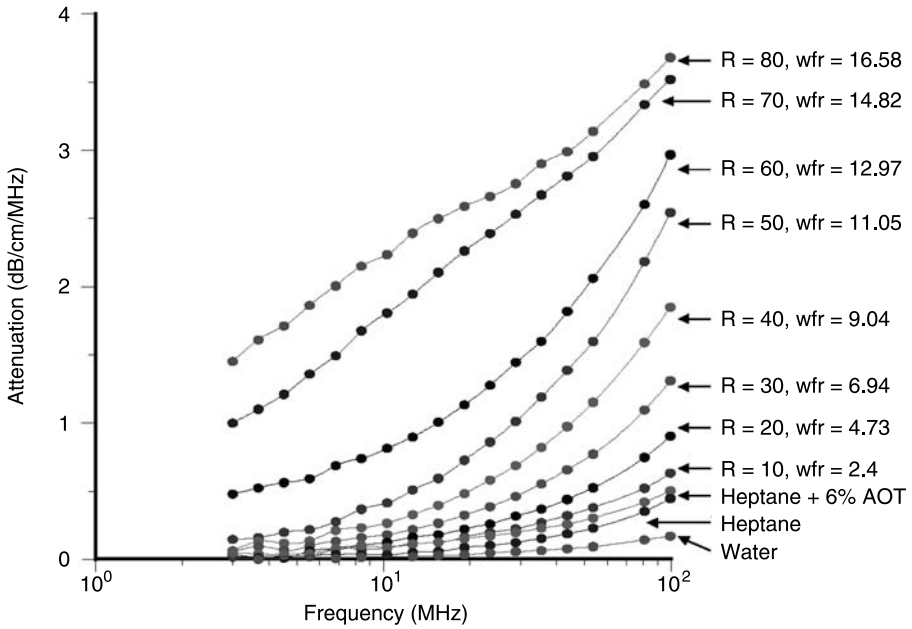

FIGURE 9.17 Acoustic attenuation spectra measured for water/AOT/heptane system for different water to AOT ratios *R*.

For *R* values > 70, an increase in the viscosity and a decrease in the reproducibility of the attenuation measurement were observed. This could be due to the failure of the model for this system as a collection of separate droplets at high R values.

A second set of experiments was run to check the reproducibility. The results of both sets of experiments up to $R = 60$ are given in Figure 9.18. It can be seen that the error related to the reproducibility is much smaller than the difference between attenuation spectra for the different *R* values. This demonstrates that the variation of attenuation reflects changes in the sample properties of water weight fraction and droplet size. The sound attenuation at *R* values above 60 were not as reproducible, but did give the same form of a bimodal distribution as the best fit for the experimental data.

The two lowest attenuation curves correspond to the attenuation in the two pure liquids: water and heptane. This attenuation is associated with oscillation of liquid molecules in the sound field. If these two liquids are soluble in each other, the total attenuation of the mixture would lie between these two lowest attenuation curves. But it can be seen that the attenuation of the mixture is much higher than that of the pure liquids. The increase in attenuation, therefore, is due to this heterogeneity of the water in the heptane system. The extra attenuation is caused by motion of droplets, not separate molecules. The scale factor (size of droplets) corresponding to this attenuation is much higher than that for pure liquids (size of molecules).

The current system contains a third component – AOT. A question arises on the contribution of AOT to the measured attenuation. In order to answer this question, measurements were done on a mixture of 6.1% wt AOT in heptane ($R = 0$). It is the third smallest attenuation curve on Figure 9.17. It is seen that attenuation increases somewhat due to AOT. However, this increase is less than the extra attenuation produced by water droplets. The small increase in attenuation

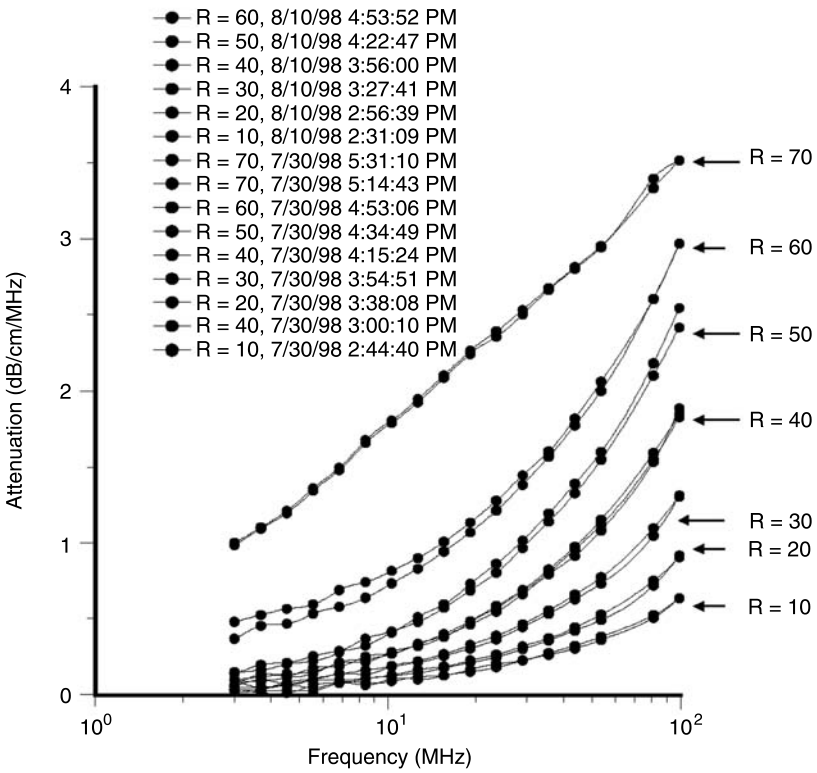

FIGURE 9.18 Reproducibility test of the attenuation measurement.

is attributed to AOT micelles. Unfortunately thermal properties of the AOT as a liquid phase are not known and the size of these micelles could not be calculated.

The droplet size distributions corresponding to the measured attenuation spectra are presented in Figure 9.19. It can be seen that the distribution becomes bimodal for $R \geq 60$ that coincides with the onset of turbidity. It is to be noted that such a conclusion could not easily be arrived at with other techniques. However, Figure 9.19 illustrates a peculiarity of this system that can be compared with independent data from literature: mean particle size increases with R almost in a linear fashion. This dependence becomes apparent when mean size is plotted as a function of R as in Figure 9.20.

It is seen that mean particle size measured using acoustic spectroscopy is in good agreement with those obtained independently using the neutron scattering (SANS) and X-ray scattering (SAXS) techniques [29,35] for R values ranging from 20 to 60. A simple theory based on equi-partition of water and surfactant can reasonably explain the observed linear dependence.

At $R = 10$ the acoustic method gave a slightly larger diameter than expected. This could be due to the constrained state of the "bound water" in the swollen reverse micelles. The water under these conditions may exhibit different thermal properties than the bulk water used in the particle size calculations. Also at the low R values ($R \leq 10$ or $\leq 2.4\%$ water), the attenuation spectrum is not very large as compared to the background heptane signal. Contribution of droplets to attenuation spectrum then may become too low to be reliably distinguished from the background signal coming from heptane molecules and AOT micelles.

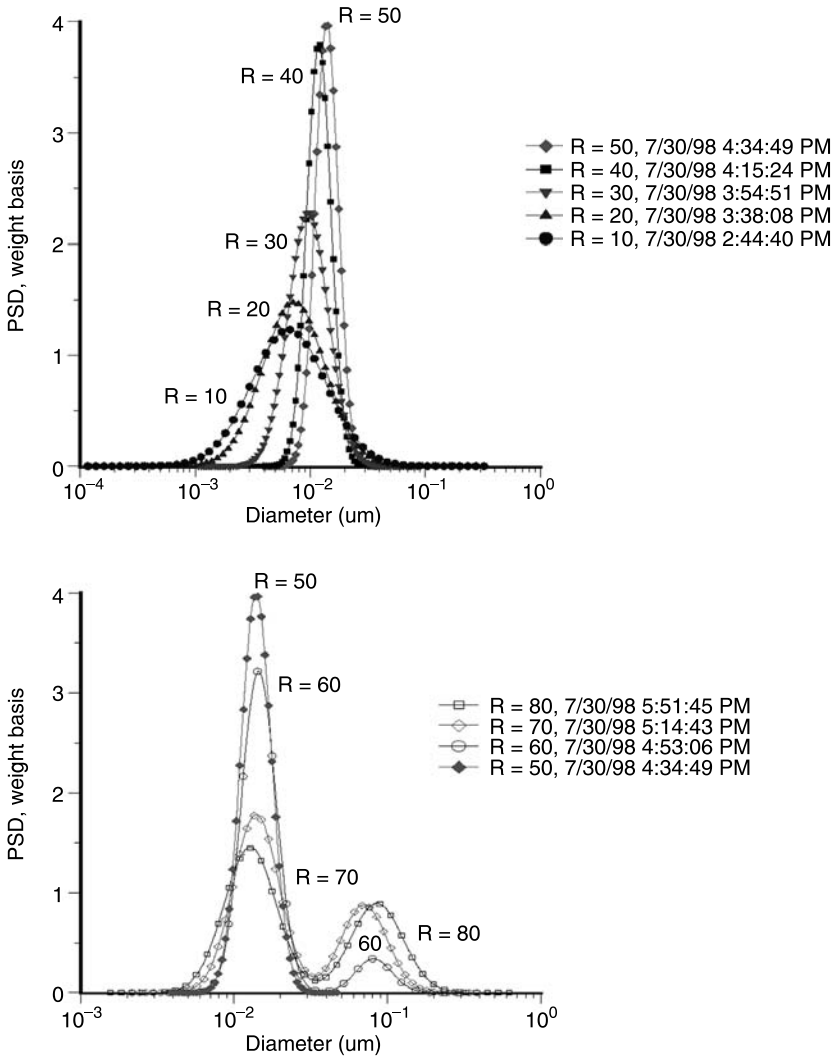

FIGURE 9.19 Drop size distribution for varying R [H_2O]/[AOT] from 10 to 50 and from 50 to 80.

9.4.4 Evolution of Water-in-Oil Emulsion Controlled by Droplet–Bulk Ion Exchange

This section describes interesting observations made while working with water-in-kerosene emulsion stabilized with nonionic surfactant. This emulsion exhibits time evolution of the acoustic and electric properties. These results have been published in *Colloids and Surfaces* [44].

We used the surfactant sorbitan mono-oleate, known also as SPAN 80 (Fluka), at surfactant contents of 0.5%, 1%, and 5% by weight relative to kerosene. The system with 1% is the most convenient for illustrating the observed effects. We used kerosene of different origins available at hardware stores. The origin of the kerosene had practically no influence on the results of measurements. We used a value of 2 for the dielectric constant of kerosene because it is not clear how impurities would affect this number. We used distilled water and water with 0.01 M KCl.

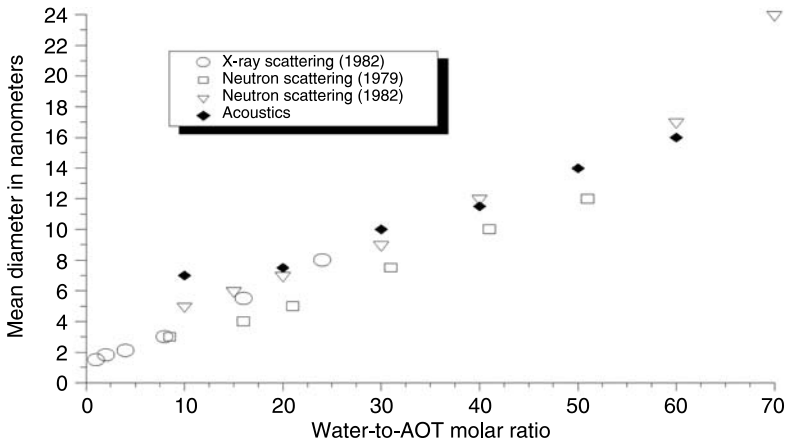

FIGURE 9.20 Comparison of mean droplet size measured using acoustic spectroscopy, neutron scattering, and X-ray scattering.

For the preparation of emulsions, water is added to the kerosene solution with a certain concentration of the SPAN. Then this solution is sonicated for 2 min. The water content is 5% vol in all samples. The droplet size of water in the kerosene emulsions was measured using the DT-1200 by Dispersion Technology. The average measurement time for these samples is about 6 min. These emulsions require continuous mixing to prevent settling, which is provided by the built-in magnetic stirrer bar in the DT-1200 sample chamber.

Kerosene evaporates if the chamber remains open and it is important to prevent this during acoustic measurements because a variable gap between the transducer and receiver causes a variation in the volume of the internal chamber over time. In order to minimize this effect the top of the chamber is covered with a flexible latex glove that could expand and contract during the measurement.

For conductivity measurements we used a Model 627 Conductivity Meter by Scientifica. It operates at 18 Hz with an applied voltage of about 5 V rms. The measurement range is 20 to 20,000 pS/cm. A Zeta Potential Probe DT-300 was used for electroacoustic measurement.

Preventing the evaporation of kerosene during conductivity–electroacoustic measurement is more complicated because of the conductivity probe structure. This probe consists of the two co-centric cylinders. Flow of liquid should move through the probe, which is inserted into the DT-1200 chamber from the top. A connecting cable causes a problem when we attempt to create an airtight seal. In addition, kerosene vapor affects the properties of the sealant. As a result we can only keep the chamber sealed for a restricted amount of time, which is shorter than in the case of acoustic measurement.

We tested reproducibility of the observed effect by repeating the same experiment several times. Altogether we made 4313 measurements from December 2003 through April 2004. We present some of these repeated runs below.

The attenuation frequency spectrum is the raw data for calculating the droplet size distribution. Figure 9.21 shows the attenuation curve as it evolves in time. Figure 9.22 illustrates just trends using a simpler two-dimensional presentation. It indicates that low frequency attenuation begins to decay as soon as sonication stops. The high frequency attenuation begins to increase with a 10-h delay. This increase is the most striking feature of the process. It is quite reproducible, as shown in Figure 9.23, and occurs at different water and surfactant contents.

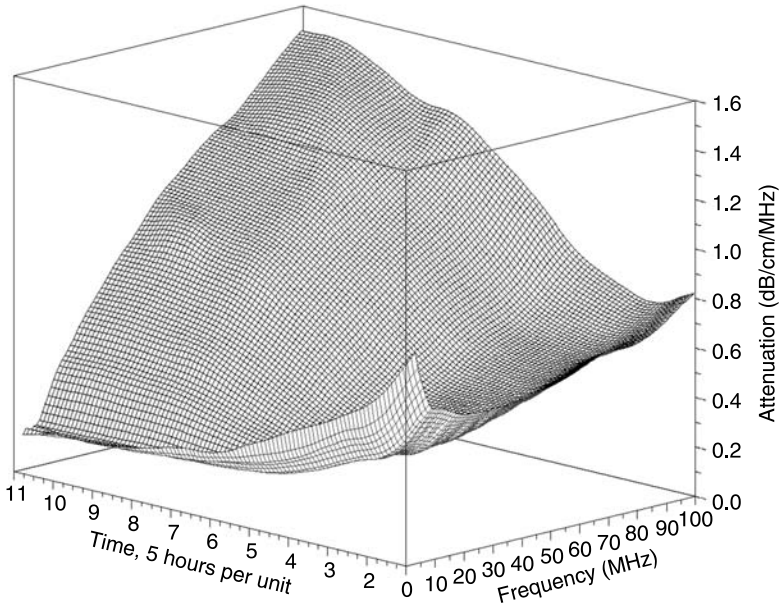

FIGURE 9.21 Attenuation frequency spectra evolution in time.

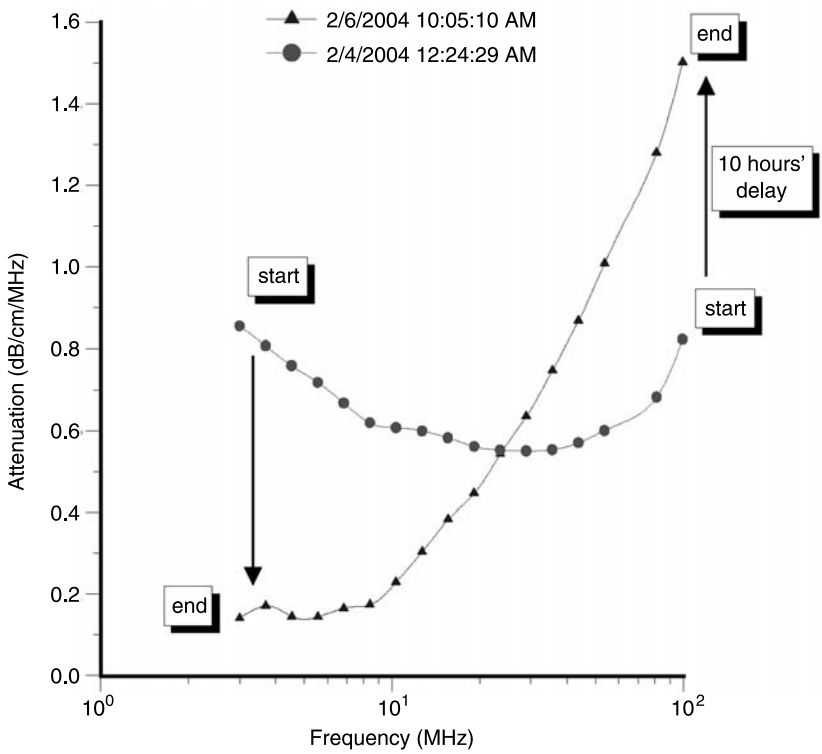

FIGURE 9.22 Attenuation frequency spectra at the beginning and at the end of experiment. Arrows show trends in attenuation evolution.

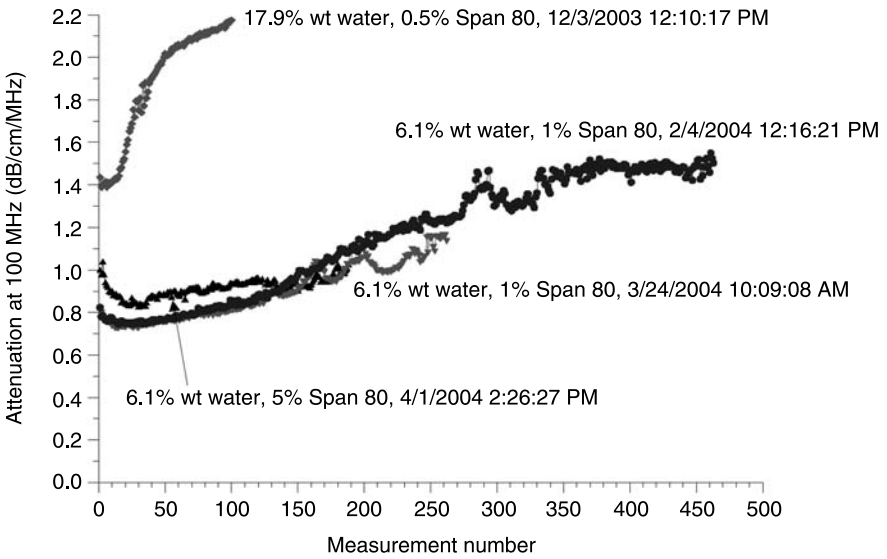

FIGURE 9.23 Evolution of the attenuation at 100 MHz in time for various emulsions. Reproducibility test with 6.1% wt water-in-kerosene emulsion with one percent of Span 80.

This evolution of the attenuation spectra reflects the variation of the droplet size distribution. Figure 9.24 presents the droplet size distribution calculated at 5-h intervals. Table 9.2 presents input parameters that are required for performing this calculation.

It is seen that during the first 10 h the droplet size increases monotonically, corresponding to simple coalescence of the original emulsion droplets. During this initial period the median droplet size changes roughly from 0.4 to 2 microns.

Then, suddenly, after 10 h a fraction with an average size of 25 nm appears. The content of this fraction increases during the next 30 h. The emulsion fraction continues to coalesce during this time, eventually reaching a size of about 7 microns.

The third period in the emulsion evolution begins roughly after 40 h. At this point the emulsion converts completely to the small size state. After this the attenuation spectra become stable and evolution of the droplet size stops.

Comparison of these droplet size distributions with attenuation spectra reveals a very simple correlation. The attenuation at low frequencies below 10 MHz corresponds to the emulsion droplets, whereas the small size droplets contribute to the high frequency attenuation.

Droplet size distributions in Figure 9.24 are the result of automatic calculation performed by DT-1200 software. It interprets attenuation as a combination of intrinsic losses and thermal losses. Intrinsic losses are independent of the droplet size. It is simple volume averaged ultrasound attenuation in homogeneous materials of the dispersed phase and dispersion medium. Thermal losses are droplet size sensitive.

Figure 9.25 presents the contribution of these two attenuation mechanisms to the last attenuation from the set presented in Figure 9.21. It is seen that theoretical attenuation fits the experiment pretty well, with a fitting error of 5.6%. This fitting corresponds to the log–normal droplet size distribution with the median size 17 nm and standard deviation 0.22.

In principle, there is another possibility for high frequency attenuation interpretation. It might be related to the scattering losses, instead of the thermal losses. In this case calculation would

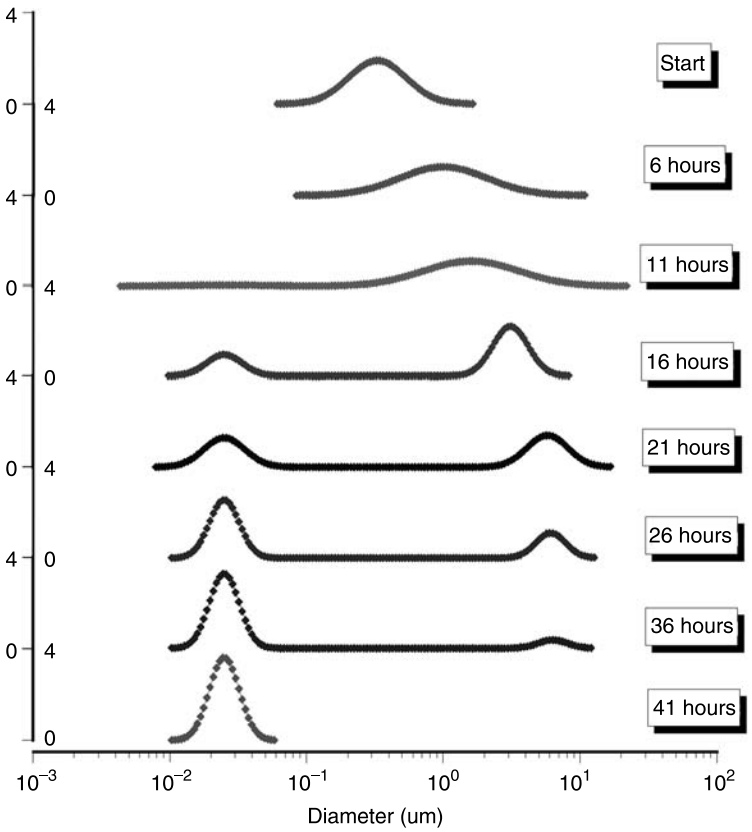

FIGURE 9.24 Evolution of the droplet size distribution in time.

TABLE 9.2
Thermodynamic Properties of the Kerosene and Water Phases Around Room Temperature

	Density (g/cm^3)	Thermal conductivity (J/m s K)	Heat capacity (J/kg K)	Thermal expansion (10^{-4} K^{-1})	Attenuation (dB/cm/MHz) – frequency (MHz)
Water	0.997	0.61	4.18	2.07	$\alpha = 0.002\omega$
Kerosene	0.81	0.15	2.85	10.6	$\alpha = 0.0106\omega$

yield a larger droplet size with increasing high frequency attenuation. It is important to clarify why DT-1200 software ignored this option and selected thermal effect over scattering. We could answer this question by forcing a searching routine in the DT-1200 software into the particular range of large sizes above 5 microns.

The best solution in this range and corresponding theoretical fitting are shown in Figure 9.26. The best median droplet size is 11.7 microns. This droplet size distribution yields theoretical attenuation that fits experimental data with error of 21.6%. This error is much larger than in the case of the thermal attenuation assumption (5.6%). This is the reason why DT-1200 software

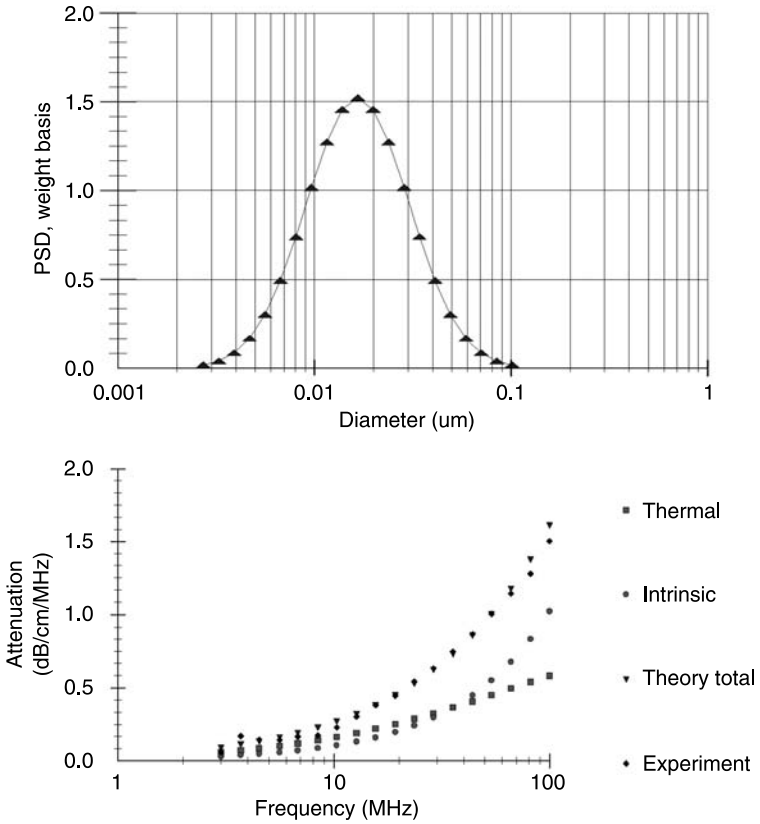

FIGURE 9.25 Droplet size of the final mini-emulsion and corresponding experimental and theoretical attenuation spectra. Droplet size does not reflect small amount of large droplets because attenuation spectra does not contain enough information for its determination.

selected small droplet size with a corresponding thermal mechanism over larger droplet sizes with a scattering mechanism.

At the same time, a combination of intrinsic and thermal attenuation for only small droplets does not provide a perfect fit. It is our experience that a fitting error of 5.6% is still quite large. We think that it happens because of the presence of a small fraction of large droplets. This could explain the leveling of the attenuation curve at low frequency as shown in Figure 9.3 for the curve marked "end." Instead of becoming practically 0 at low frequency it becomes stable at the level of about 0.1 dB/cm/MHz when the frequency is below 10 MHz. It is a clear indication of the larger emulsion droplets. Unfortunately, this attenuation is not sufficient to determine the size and amount of these droplets. That is why DT-1200 software has simply ignored them. The inability to perfectly fit this part of the attenuation spectra determines the relatively large fitting error of 5.6%.

We would like to stress the importance of being able to collect attenuation data over a wide frequency range. The absence of frequency data below 20 MHz would simply miss the variation of the emulsion fraction. Similarly, the absence of high frequency data would miss the variation due to the small size fraction.

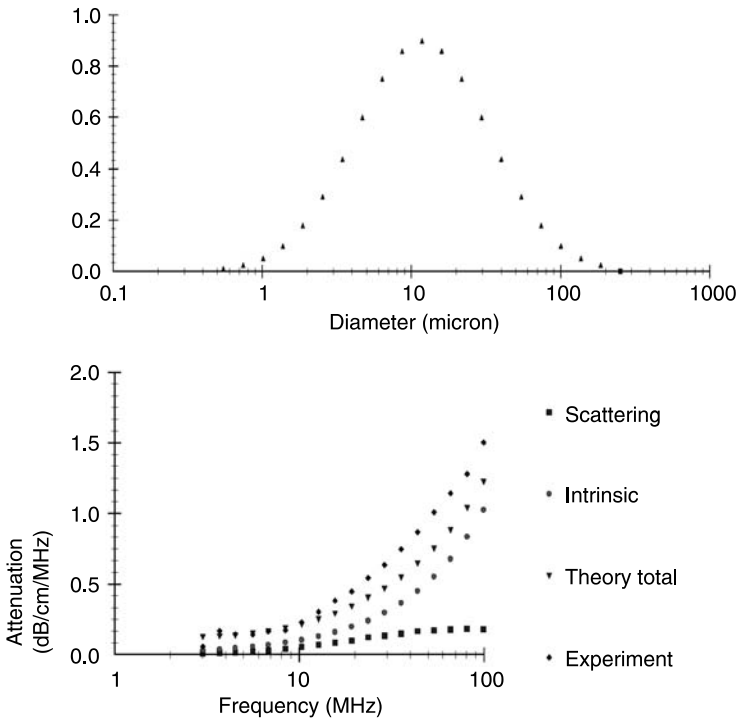

FIGURE 9.26 The best droplet size distribution assuming scattering mechanism of ultrasound attenuation. Corresponding theoretical attenuation that fail to fit experimental data.

At this point in the discussion we do not know the nature of the small droplets: they might be either microemulsion or mini-emulsion droplets. Sedimentation analysis and image analysis are used to answer this question. In addition, the reason for the strange kinetic behavior is not known. Next we will consider electroacoustic measurements to help obtain these answers, because it yields information about the surface properties of the water droplets.

The evolution of the emulsion described above occurs under conditions of continuous stirring. We use a magnetic stirrer to prevent sedimentation of the original emulsion. If we turn the stirrer off after the system reaches a steady state, the water droplets sediment. If the system was a thermodynamically microemulsion, we would observe no sedimentation effect. Hence sedimentation points toward a thermodynamically unstable mini-emulsion. This mini-emulsion turns into a sedimenting emulsion when the stirrer is turned off. At the same time there is no phase separation. If we turn the stirrer on again, the system exhibits the same acoustic properties as before sedimentation occurred with the same small droplet size. These observations indicate that we are dealing with an unstable mini-emulsion, which undergoes coalescence after stirring is turned off.

We performed two tests to confirm this conclusion. First we compared acoustic properties of this unstable system with acoustic properties of another water-in-oil emulsion, which becomes definitely microemulsion after adding surfactant. It is water-in-car oil with AOT as stabilizer. Water in pure car oil builds up an emulsion when sonicated, even without any additional surfactant. We prepared such an emulsion at 5% vol by applying 1 min of sonication. The final

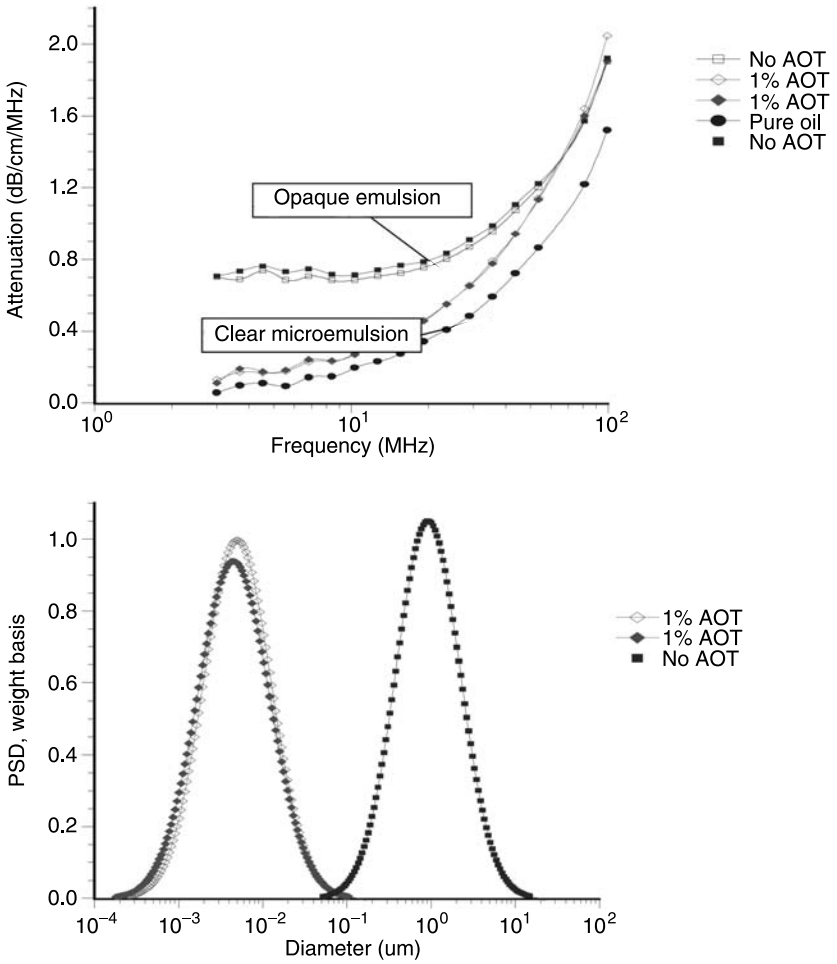

FIGURE 9.27 Attenuation spectra of 5% vol water-in-car-oil emulsion and microemulsion stabilized with 1% AOT. Corresponding droplet size distributions.

emulsion has a white color, which is specific for emulsions. It indicates very high turbidity, which is usually associated with droplet sizes of the order of microns. The attenuation spectra and corresponding droplet size for this emulsion are shown in Figure 9.27. The median size is about 2 microns, as expected.

At the second stage of this experiment we added 1% of AOT to this emulsion. After 1 min of sonication this liquid becomes transparent with a color practically identical to the color of the original car oil. This simple observation is definite proof that AOT converts emulsion into microemulsion. Figure 9.27 shows that acoustic properties have changed dramatically as well. Attenuation becomes much smaller and the median droplet size becomes about 10 nm. This experiment shows that there is a clear correlation between acoustics and optical properties of the stable emulsion–microemulsion transition.

We could now compare attenuation spectra of water-in-kerosene emulsion (Figure 9.22) with water-in-car-oil emulsion (Figure 9.27). There is clear similarity between these curves. We know

that the low attenuation curve in the case of water-in-car-oil corresponds to the stable and optically transparent microemulsion. This could be used as justification for our earlier conclusion that lower attenuation at low frequency is indication of the smaller droplet sizes in the case of water-in-kerosene emulsion at the final stages of its evolution.

Unfortunately, the optical test in the case of the water-in-kerosene emulsion is not as definite as in the case of the water-in-car-oil emulsion. The water-in-kerosene emulsion remains opaque independently on variation of the acoustic properties. However, it is not sufficient to claim that there are no small mini- or microemulsion droplets in the system at the end of its evolution. A small amount of larger droplets could be responsible for the high turbidity.

In order to verify this hypothesis we performed a microscopic analysis of the final system after 40 h of stirring. We used a dark field microscope with a digital camera to capture images continuously for 1 h. Figure 9.28 shows five snapshots of the emulsion image at intervals of 10 min. It is clearly seen that the size of the emulsion droplets grows with time. However, the large droplets of micron size do not coalesce. The growth that we observe is apparently related to

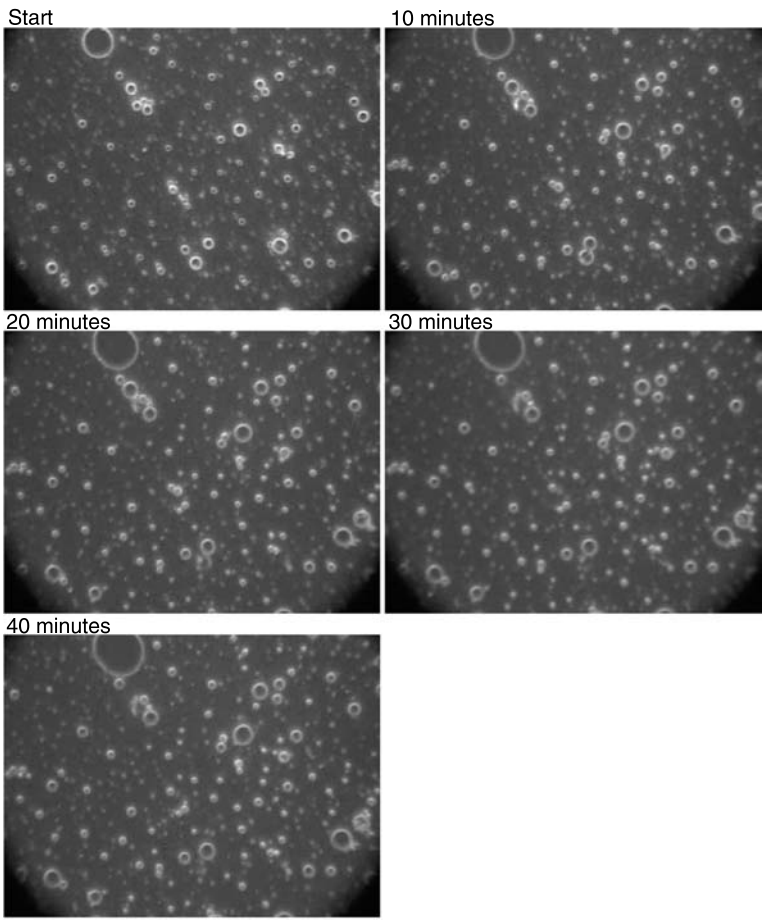

FIGURE 9.28 Emulsion evolution after stirrer is turned off. The width of each picture is approximately 100 microns.

the capturing of the very small droplets by the larger ones. These small droplets look like bright dots in the dark field. Microscopy does not allow estimate of their sizes, which are clearly less than a micron.

This microscopic test confirmed that the system contains a number of very small droplets, which slowly coalesce in larger droplets with a higher degree of aggregative stability. Stirring breaks quickly these large droplets into the smaller ones. These small mini-emulsion droplets dominate the acoustic attenuation, which is measured under stirring conditions.

At the same time it confirms presence of larger droplets with sizes on micron scale. This is the fraction that contributes 0.1 dB/cm/MHz to the low frequency attenuation in Figure 9.22, curve "end." Apparently volume fraction of these large droplets is not sufficient for being reflected in the droplet size distributions calculated from the attenuation spectra.

The presence of this small fraction of larger droplets could explain the high turbidity of the final mini-emulsion. Unfortunately, we could not estimate the amount of these larger droplets either from acoustics or from optical images. In order to detemine the cause of this interesting evolution we use electroacoustic and conductivity measurements for monitoring variation of electric properties. Electroacoustic measurement in non-aqueous systems involves three steps. First is calibration with 10% silica Ludox in 0.01 M KCl aqueous solution. The zeta potential of this dispersion is −38 mV, which is the basis for calibration.

The second step is the measurement of the electroacoustic signal of pure kerosene. This gives us the value of the background or ion vibration signal. The presence of surfactant does not affect this background signal, as shown with measuring kerosene that contains the surfactant. The DT-1200 software allows us to save this value and to subsequently subtract this background signal from further measurements. It is a vector subtraction because the electroacoustic signal is a vector with a certain magnitude and phase. As a simple test that this subtraction works, we measured kerosene again, this time making the background subtraction. This test gives us the value of the noise level of the electroacoustic measurement.

The third step is the actual measurement of the electroacoustic signal generated by the water-in-kerosene emulsion. This signal substantially exceeded the noise level, as shown in Figures 9.29 and 9.30. Figure 9.30 illustrates reproducibility of this effect.

With time, the CVC magnitude gradually decreases. Unfortunately, we are not able to measure CVC continuously during 40 h with the existing experimental setup. We mentioned before that the measuring chamber must be airtight for preventing kerosene evaporation. The cable of the conductivity probe makes this hard to achieve. Simple sealant that we use becomes affected by kerosene vapor. That is why conductivity and CVC measurement are conducted only during 20 h, as it is shown in Figures 9.9 and 9.10.

However, we are able to measure conductivity and CVC of the final emulsions as a single point measurement even days after the experiment finished. For instance, we stored emulsion after 40 h of the attenuation measurement. Later we could use this emulsion for CVC and conductivity measurement. For instance, after 8 days two consequent measurements of CVC yield values 1318 and 1973. That is why we could state that eventually CVC reaches the noise level. From this CVC behavior with time we can conclude that:

- The microemulsion droplets do not contribute to the CVC signal
- The emulsion droplets do contribute to the CVC signal

There are several ways to explain the peculiarities of this system, as follows. We can use the CVC values at the initial stage of coalescence for calculating the surface charge σ of the water droplets. According to Shilov's theory, this calculation requires certain input parameters, such as

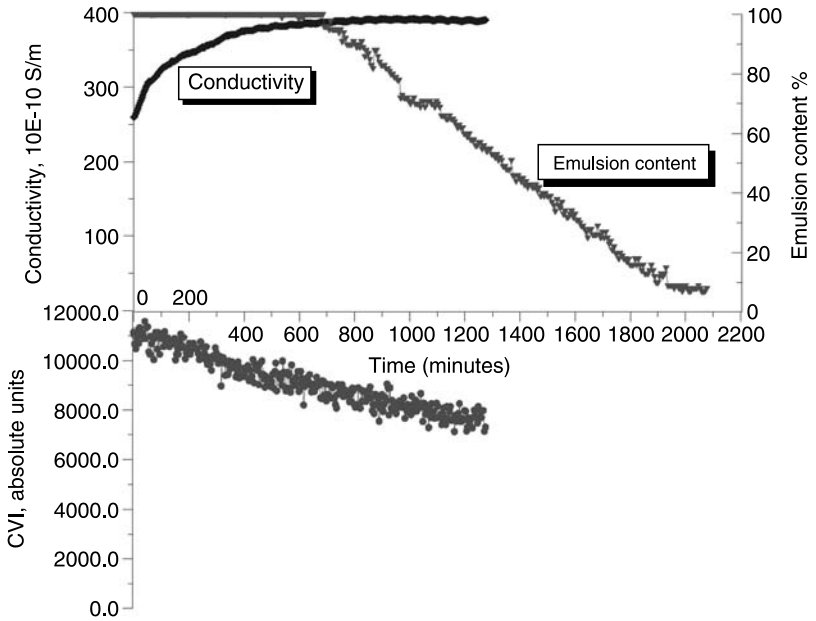

FIGURE 9.29 Correlation between emulsion droplet content and measured conductivity and electroacoustic signal.

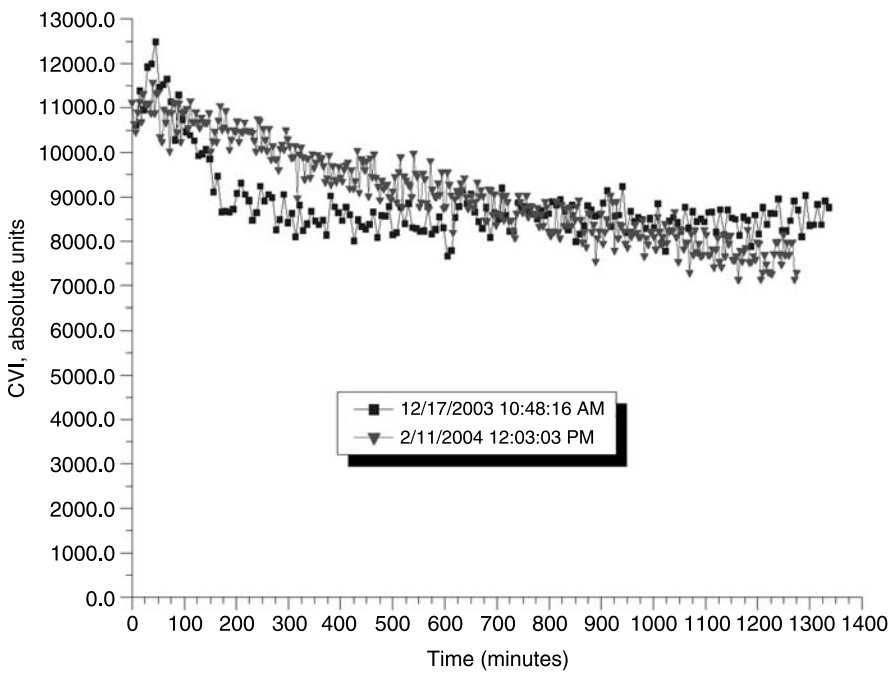

FIGURE 9.30 Illustration of reproducibility of the effect and electroacoustic measurement.

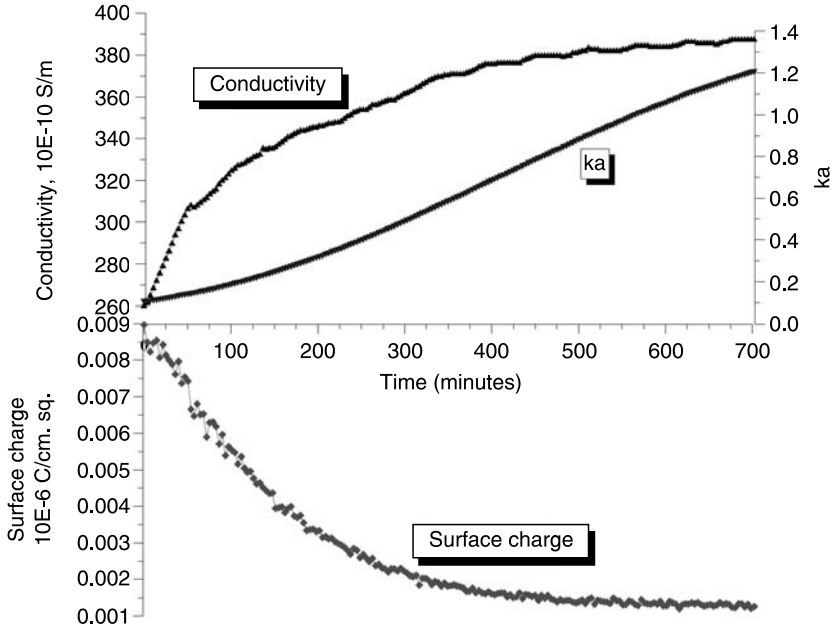

FIGURE 9.31 Correlation between measured conductivity and calculated apparent surface charge density.

the properties of liquids and the size of the water droplets. Acoustic attenuation measurements yield information about the droplet size. As for the liquid properties, we use the following values: $\rho_m = 0.8$ g/cm^3; $\rho_p = 1$ g/cm^3; $\eta = 1.5$ cp; $\varepsilon_m = 2$; $\varepsilon_p = 80$. All these parameters are corrected for temperature.

Figure 9.31 shows the resulting values for the surface charge evolution during the stage of emulsion coalescence. It is seen that it decays quickly with time, decreasing by almost 10 times during the first 10 h. Surface charge decays with time much faster than CVC (Figure 9.31) because droplet size increases almost five times during this period. Equation 9.8 indicates that dynamic mobility and accordingly CVC are proportional to the product of the surface charge by the droplet size.

The question arises about the mechanism for this effect. Does this mean that the adsorbed SPAN molecules are losing charges they carry to the surface? Is there any other explanation that would not involve restructuring of the SPAN molecules? In answering these questions we should keep in mind a clear correlation between the apparent surface charge decay and the conductivity increase, as shown in Figure 9.29. It appears that the droplets release ions into the kerosene while coalescing.

It is important to mention that the conductivity of the initial kerosene–SPAN 80 solution is about 310×10^{-10} S/m. The conductivity of the initial emulsion is less than this value. It appears that the water droplets adsorb SPAN and reduce the conductivity. However, with time the conductivity increases, eventually exceeding the initial value in the kerosene–SPAN solution (see Figure 9.29).

Conductivity measurements allow us to estimate the κa value and determine the validity of Shilov's theory in regard to this system. It is known that Shilov's theory is valid only for overlapped DLs. Figure 9.3 shows the relationship between the volume fraction and κa for

overlapped DLs. A more detailed description is given in Ref. 6. It is seen that at a volume fraction of 5% the DLs do overlap if $\kappa a < 1$. This is the range of κa values when Shilov's theory can be applied.

Figure 9.31 presents κa values calculated using the measured conductivity and the particle size computed using attenuation spectroscopy. We also assumed that there are simple small ions in the kerosene phase with an approximate diffusion coefficient of 10^{-5} cm^2/sec. If this assumption is valid, κa satisfies the condition of overlapped DLs during the complete initial period of emulsion coalescence. This is a justification for using Shilov's theory for calculating the surface charge.

We have established so far that the evolution of the water-in-kerosene emulsion with SPAN 80 as emulsifier proceeds in three distinct periods.

Period 1: the first 10 h. The water droplets are coalescing. The apparent surface charge of the droplets decays. The conductivity increases, eventually exceeding the initial value in the kerosene–SPAN solution.

Period 2: between 10 and 40 h. The mini-emulsion fraction appears and grows. The emulsion droplets continue to coalesce. The CVC continues to decay. The rate of conductivity increase is much smaller.

Period 3: after 40 h. All parameters are stable. There are no emulsion droplets. The water is in mini- and possibly microemulsion droplets. These droplets do not generate any CVC signal.

It is quite possible that there are multiple explanations of this set of facts. Here we just suggest one of them. We do not claim that it is the only one. We want to be absolutely clear that it is just one of, perhaps, several possible models. Our model is based on the assumption that the water–kerosene interface with adsorbed SPAN remains unchanged. We assume that the SPAN molecules stabilized this interface almost instantly during initial sonication and brought it to thermodynamic equilibrium. However, it is only a local equilibrium for each small element of the interface.

The part of the SPAN molecules in the bulk of the solution is responsible for the conductivity of the original kerosene–SPAN solution. It means that they carry charge, either as individual molecules, or as micelles. It is also possible that at least a fraction of the adsorbed SPAN molecules is charged and brings this charge to the surface. We assume that the electric charge of the water–kerosene interface that is associated with adsorbed SPAN molecules remains constant, time independent. Local thermodynamic equilibrium is the justification for this assumption.

We attribute the observed evolution of the parameters to ion exchange between the interior of the water droplets and the bulk of the kerosene solution. Initially the water droplets have an electro-neutral interior. Ions are trapped inside of the large water droplet at about equal amounts. The surface charge induced by adsorbed SPAN molecules is screened with an external diffuse layer in the kerosene solution. Figure 9.32 illustrates this structure.

The external diffuse layers are very thick due to the low ionic strength. They are overlapped. This gives rise to the CVC signal. We could estimate the amount of energy W_{ext} required to charge this external DL to a certain level of surface charge Q as:

$$W_{ext} = \frac{Q^2}{2C_{ext}} = \frac{Q^2}{\varepsilon_p \varepsilon_0 S \kappa_{ext}} \tag{9.13}$$

where S is the surface area, κ_{ext} is the Debye parameter for external DLs.

Obviously, there is another possibility to screen the surface charge induced by SPAN adsorption. It could be done with screening the diffuse layer inside of the particle. This second opportunity would also take a certain amount of energy, which we could estimate with the

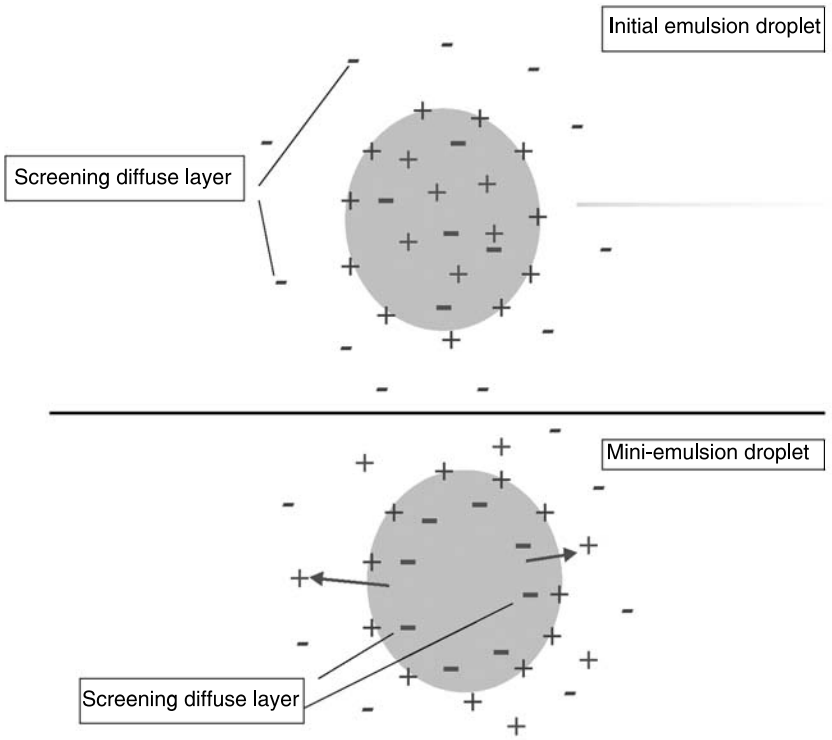

FIGURE 9.32 Illustration of the double layer restructuring due to the ion exchange between interior and exterior of the water droplet.

following equation:

$$W_{in} = \frac{Q^2}{2C_{in}} = \frac{Q^2}{\varepsilon_p \varepsilon_0 S \kappa_{in}} \tag{9.14}$$

Comparison of these two charging energies yields the following approximate result:

$$\frac{W_{in}}{W_{ext}} = \frac{\varepsilon_m \kappa_{ext}}{\varepsilon_p \kappa_{in}} = \sqrt{\frac{\varepsilon_m K_m}{\varepsilon_p K_m}} = \sqrt{\frac{K_m}{40 K_p}} \approx 0.001 \tag{9.15}$$

where we have assumed that the conductivity of water is about $10^6/40$ times larger than conductivity of kerosene, the effective diffusion coefficients D_{eff} being the same, and that the Debye parameter can be given with the following equation:

$$\kappa^2 \approx \frac{K}{\varepsilon_0 \varepsilon D_{eff}} \tag{9.16}$$

This is certainly a very approximate estimate. However, it clearly indicates that charging of the interior DL to a certain electric charge is orders of magnitude more energy efficient than the exterior one.

It is important to mention that charging up to a certain level of the electric potential, instead of the electric charge, would lead to the opposite conclusion. We believe that in this case we are dealing with the constant surface charge case because it is related to the adsorption of thermodynamically determined amount of the surfactant.

The above mentioned difference in energy for charging the DLs creates a driving force for co-ions to leave the interior of the droplet. This simply means that there is a gradient of co-ion electrochemical potential that drives co-ions from the droplet out. This statistical process is slow because the ion should become solvated by surfactant molecules on the kerosene–water interface. It is known [44] that only sufficiently large ions could exist in nonpolar liquids. This slow leakage of co-ions from the droplet generates an internal electric charge that would screen the adsorbed surface charge. Eventually this would lead to the complete collapsing of the external DL. The surface charge of the adsorbed SPAN would be completely compensated by the interior charge of the water droplet. Figure 9.12 illustrates this final stage of the transition.

This model could explain all observed features of the emulsion–mini-emulsion transition. First, it explains why the conductivity increases during the coalescence period and eventually significantly exceeds the conductivity level of the original kerosene–SPAN solution (see Figure 9.29). This excess conductivity comes from the counter-ions released from the water droplets into the kerosene.

An alternative model that could potentially explain some of the observed facts with restructuring of the adsorbed SPAN molecules would not explain the excess conductivity. This is a serious argument supporting the "ion exchange model."

The "ion exchange model" also explains the lack of the CVC signal for the microemulsion. It happens because the surface charge of the adsorbed SPAN molecules is completely screened with the internal charge of the microemulsion droplet. Consequently it looks from the outside as being electro-neutral.

In this model redistributing screening electric charge from the outside diffuse layer to the inside one is a limiting factor of the emulsion droplet break up into much smaller mini- and possibly microemulsion droplets. Apparently this break up occurs when a sufficient critical amount of energy is released due to the collapsing external DL.

Another potential factor controlling this break-up, droplet size, does not seem to be important. We could conclude this based on the observation that the size of the emulsion droplets continues to grow during period 2. If break-up was related to the droplet size, we would observe growth only up to a certain maximum value of the size. This is obviously not the case.

This break-up is not exactly spontaneous because it strongly depends on the presence of stirring. However, stirring with a magnetic stirrer bar in the DT-1200 chamber is not vigorous. It is clear that reduction of the surface tension is a most important factor. In this sense the observed phenomenon is similar to the "negative interfacial tension" mechanism of spontaneous emulsification. It is also possible that the combination of stirring and reduction of the surface tension intensifies "interfacial turbulence."

Finally, we would like to repeat that the suggested mechanism explains all the experimental facts, but we could not claim that it is the only one to do so. There might be some other explanations of the phenomenon presented in this paper.

REFERENCES

1. Pellam, J.R. and Galt, J.K. "Ultrasonic propagation in liquids: Application of pulse technique to velocity and absorption measurement at 15 megacycles", *J. Chem. Phys*. **14**(10), 608–613 (1946).

2. Sewell, C.T.J. "The extinction of sound in a viscous atmosphere by small obstacles of cylindrical and spherical form", *Phil. Trans. Roy. Soc., Lond*. **210**, 239–270 (1910).
3. Epstein, P.S. and Carhart, R.R. "The absorption of sound in suspensions and emulsions", *J. Acoust. Soc. Amer*. **25**(3), 553–565 (1953).
4. McClements, D.J. "Ultrasonic characterization of emulsions and suspensions", *Adv. Colloid Interface Sci*. **37**, 33–72 (1991).
5. "Ultrasonic and Dielectric Characterization Techniques for Suspended Particulates", V.A. Hackley and J. Texter (Eds), The American Chemical Society, Ohio (1998).
6. Dukhin, A.S. and Goetz, P.J. "Ultrasound for Characterizing Colloids. Particle Sizing, Zeta Potential, Rheology", New York, Elsevier (2002).
7. Lyklema, J. "Fundamentals of Interface and Colloid Science", Volume 1, Academic Press (1993).
8. Hunter, R.J. "Foundations of Colloid Science", Oxford University Press, Oxford (1989).
9. Hunter, R.J. "Review. Recent developments in the electroacoustic characterization of colloidal suspensions and emulsions", *Colloids and Surfaces* **141**, 37–65 (1998).
10. Strout, T.A. "Attenuation of sound in high-concentration suspensions: development and application of an oscillatory cell model", Thesis, University of Maine (1991).
11. Allegra, J.R. and Hawley, S.A. "Attenuation of sound in suspensions and emulsions: theory and experiments", *J. Acoust. Soc. Amer*. **51**, 1545–1564 (1972).
12. McClements, D.J. "Ultrasonic determination of depletion flocculation in oil-in-water emulsions containing a nonionic surfactant", *Colloids and Surfaces* **90**, 25–35 (1994).
13. McClements, D.J. "Comparison of multiple scattering theories with experimental measurements in emulsions", *J Acoust. Soc. Amer*. **91**(2), 849–854 (1992).
14. Holmes, A.K., Challis, R.E. and Wedlock, D.J. "A wide-bandwidth study of ultrasound velocity and attenuation in suspensions: Comparison of theory with experimental measurements", *J. Colloid Interface Sci*. **156**, 261–269 (1993).
15. Holmes, A.K., Challis, R.E. and Wedlock, D.J. "A wide-bandwidth ultrasonic study of suspensions: The variation of velocity and attenuation with particle size", *J. Colloid Interface Sci*. **168**, 339–348 (1994).
16. Dukhin, A.S., Goetz, P.J. and Hamlet, C.W. "Acoustic spectroscopy for concentrated polydisperse colloids with low density contrast", *Langmuir* **12**(21), 4998–5004 (1996).
17. Anson, L.W. and Chivers, R.C. "Thermal effects in the attenuation of ultrasound in dilute suspensions for low values of acoustic radius", *Ultrasonic* **28**, 16–25 (1990).
18. Dukhin, A.S. and Goetz, P.J. "Acoustic spectroscopy for concentrated polydisperse colloids with high density contrast", *Langmuir* **12**(21), 4987–4997 (1996).
19. Harker, A.H. and Temple, J.A.G. "Velocity and attenuation of ultrasound in suspensions of particles in fluids", *J. Phys. D., Appl. Phys*. **21**, 1576–1588 (1988).
20. Gibson, R.L. and Toksoz, M.N. "Viscous attenuation of acoustic waves in suspensions", *J. Acoust. Soc. Amer*. **85**, 1925–1934 (1989).
21. Riebel, U., et al. "The fundamentals of particle size analysis by means of ultrasonic spectrometry", *Part. Part. Syst. Charact*. **6**, 135–143 (1989).
22. Chanamai, R., Coupland, J.N. and McClements, D.J. "Effect of temperature on the ultrasonic properties of oil-in-water emulsions", *Colloids and Surfaces* **139**, 241–250 (1998).
23. Temkin, S. "Sound speed in suspensions in thermodynamic equilibrium", *Phys. Fluids* **4**(11), 2399–2409 (1992).
24. Temkin, S. "Sound propagation in dilute suspensions of rigid particles", *The Journal of the Acoustical Society of America*. **103**(2), 838–849 (February 1998).
25. O'Brien, R.W. "Electro-acoustic effects in a dilute suspension of spherical particles", *J. Fluid Mech*. **190**, 71–86 (1988).
26. O'Brien, R.W. "Determination of particle size and electric charge", US Patent 5,059,909 (22 October 1991).
27. Dukhin, A.S., Ohshima, H., Shilov, V.N. and Goetz, P.J. "Electroacoustics for concentrated dispersions", *Langmuir* **15**(10), 3445–3451 (1999).
28. Dukhin, A.S., Shilov, V.N, Ohshima, H. and Goetz, P.J. "Electroacoustics phenomena in concentrated dispersions. New theory and CVI experiment", *Langmuir* **15**(20), 6692–6706 (1999).

29. Dukhin, A.S., Shilov, V.N, Ohshima, H. and Goetz, P.J. "Electroacoustics phenomena in concentrated dispersions. Effect of the surface conductivity", *Langmuir* **16**, 2615–2620 (2000).
30. Shilov, V.N., Borkovskaja, Yu.B. and Dukhin, A.S. "Electroacoustic theory for concentrated colloids with arbitrary κa. Nano-colloids. Non-aqueous colloids", *J. Colloid Interface Sci.* **277**, 347–358 (2004).
31. Dukhin, A.S. and Goetz, P.J. "Characterization of concentrated dispersions with several dispersed phases by means of acoustic spectroscopy", *Langmuir* **16**(20), 7597–7604 (2000).
32. Dukhin, A.S., Goetz, P.J. and Truesdail, S.T. "Surfactant titration of kaolin slurries using ζ-potential probe", *Langmuir* **17**, 964–968 (2001).
33. Crupi, V., Maisano, G., Majolino, D., Ponterio, R., Villari, V. and Caponetti, E. *J. Mol. Struct*. **383**, 171 (1996).
34. Bedwell, B. and Gulari, E. In: "Solution Behavior of Surfactants" (K.L. Mittal, Ed.), Vol. 2., Plenum Press, New York (1982).
35. Gulari, E., Bedwell, B. and Alkhafaji, S. *J. Colloid Interface Sci*. **77**(1), 202 (1980).
36. Zulauf, M. and Eicke, H.-F., *J. Phys. Chem*. **83**(4), 480 (1979).
37. Eicke, H.-F. In: "Microemulsions" (I.D. Rob, Ed.), p. 10, Plenum Press, New York (1982).
38. Nicholson, J.D., Doherty, J.V. and Clarke, J.H.R. In: "Microemulsions" (I.D. Rob, Ed.), p. 33, Plenum Press, New York (1982).
39. Eicke, H.-F. and Rehak, J. *Helv. Chim. Acta* **59**(8), 2883 (1976).
40. Radiman, S., Fountain, L.E., Toprakcioglu, C., de Vallera, A. and Chieux, P. *Progr. Coll. Polym. Sci.* **81**, 54 (1990).
41. Fletcher, P.D.I., Robinson, B.H., Bermejo-Barrera, F., Oakenfull, D.G., Dore, J.C. and Steytler, D.C. In: "Microemulsions" (I.D. Rob, Ed.), p. 221, Plenum Press, New York (1982).
42. Cabos, P.C. and Delord, P. *J. App. Cryst*. **12**, 502 (1979).
43. Dukhin, A.S. and Goetz, P.J. "New developments in acoustic and electroacoustic spectroscopy for characterizing concentrated dispersions", *Colloids and Surfaces* **192**, 267–306 (2001).
44. Dukhin, A.S. and Goetz, P.J. "Evolution of water-in-oil emulsion controlled by droplet-bulk ion exchange: acoustic, electroacoustic, conductivity and image analysis", *Colloids and Surfaces* (2004).